Highlights

- Joint temperature is considerably reduced in the fire situation

- Regions close to steel tube show a significant moisture plateau

- FEA model using Eurocode 4 thermal properties gives satisfactory predictions

Experimental and numerical study of temperature developments of composite joints between concrete-encased concrete-filled steel tube columns and reinforced concrete beams

Kan Zhou[a,b1], Lin-Hai Han[a]

[a] Department of Civil Engineering, Tsinghua University, Beijing, 100084, China.
[b] Faculty of Engineering and Informatics, University of Bradford, Bradford, West Yorkshire, BD7 1DP, UK.

Abstract: Previous studies of concrete-encased concrete-filled steel tube (CFST) columns have demonstrated their enhanced fire performance due to the passive protection of the outer encasement. To facilitate the design and application of concrete-encased CFST structures, the fire performance of full-scale reinforced concrete beam to concrete-encased CFST column joints subjected to full-range fire including heating and cooling phases was studied experimentally. This paper presents the experimental programme and reports the experimental results related to temperature. Finite element analysis (FEA) models of varying complexities were also incorporated to complement the fire tests and to better interpret the temperature developments. Results show that beam failure was observed for all tested specimens. Concrete explosive spalling was insignificant due to the low strength of the outer concrete. The temperature of the joint zone was tremendously reduced compared to the connected members due to the passive protection of outer concrete and the heat sink effect. The temperature-time curves of the region close to the steel tube showed a significant moisture plateau. The FEA models produced satisfactory temperature predictions when the thermal properties in Eurocode 4 were used.

Keywords: concrete-encased steel section; joint; composite column; concrete-filled steel tube; reinforced concrete; heat transfer; temperature; cooling phase; post-fire.

---

[1] corresponding author, k.zhou1@bradford.ac.uk.

Notation

a	Thickness of the ceramic fibre blanket
B_c	Width of the concrete-encased CFST cross-section
b	Width of the cross-section of the beam
D	Outer diameter of the steel tube/reinforcement bars
D_c	Depth of the concrete-encased CFST cross-section
E_s	Modulus of elasticity of steel
f_y	Yield strength of steel
f_u	Ultimate strength of steel
h	Height of the cross-section of the beam
N	Load
N_f	Load applied to the column in the fire situation
P_f	Load applied to the beam in the fire situation
t	Time, or length of the plateau in the temperature-time curve
t_h	Duration of fire exposure or heating phase
t_o	Heating time ratio, $=t_h/t_R$
t_R	Fire resistance
t_s	Wall thickness of the steel tube
u	Moisture content
θ	Temperature, in °C
θ_c	Temperature calculated by the numerical methods, in °C
θ_e	Temperature measured in the experiment, in °C
$\theta_{f,ave}$	Average furnace temperature, in °C
θ_{max}	Maximum temperature attained during the heating phase and the subsequent cooling phase, in °C
ν_s	Poisson's ratio

1. Introduction

Concrete-encased concrete-filled steel tube (CFST) columns, comprised of an inner encased CFST component and an outer encasing reinforced concrete (RC) component, are a type of composite steel-concrete structures. Benefiting from the composite action, they can achieve high load-carrying capacity and exceptional seismic performance. Besides, a preliminary experimental study has demonstrated that they are able to achieve exceptional fire resistance and enhanced post-fire residual strength, as compared with conventional CFST columns [1]. A follow-up numerical study confirms the composite action between the outer RC component and the inner CFST component in the fire situation [2].

Although these studies have paved the way for a rational fire design method for concrete-encased CFST columns, research results based on isolated column members might not reflect the behaviour of an entire structure due to a lack of structural continuity. In the fire situation, joints could develop a different temperature profile as compared with the connected members, and thus might behave in a different manner. Also, the compressive force developing in restrained beams during heating and the tensile force during cooling may affect the behaviour of the joints [3]. Although joints could attain a lower temperature in the fire situation than the connected members due to the shielding effect, the additional forces acting at the joints during heating and cooling could outweigh that of the advantage resulting from the shielding effect [4]. Therefore, it is also essential to study the behaviour of the joints that connect concrete-encased CFST columns. An experimental study of the fire behaviour of isolated joints will establish a preliminary knowledge and provide precious experimental data.

Extensive studies on the fire behaviour of beam-to-column joints are available, as reviewed in refs. [5]-[8]. The study on joint behaviour initially focused on steel joints using various types of connections, at both the connection level and the beam-to-column subassembly level. Then it started to cover a

3

wider range of composite steel-concrete joints, such as the joints connecting composite beams [9]-[10], composite columns [11]-[15] and combinations of them [16]-[18]. Studies on the behaviour of joints and frames subjected to seismic action and fire are also available [19]-[21]. Since concrete-encased CFST structures were initially designed to achieve exceptional seismic resistance, more attention has been paid to their seismic performance [22]-[24]. Recently, their fire performance has been addressed; but at column level only [1][2]. Their performance at joint level has yet to be understood. To close this research gap, an experimental investigation has been performed to examine the fire performance of concrete-encased CFST composite joints.

In practice, concrete-encased CFST columns can be versatile; it is feasible to connect them with RC beams, steel beams and composite beams. This study sets out to test the composite joints between concrete-encased CFST columns and RC beams. The reasons why RC beam was selected in the joint configurations were that: (1) concrete-encased CFST columns are commonly connected with RC beams or composite beams in construction practice; and (2) concrete-encased CFST columns are more susceptible to a premature failure in such configurations than those connected with steel beams. Additionally, conducting the fire tests of composite joints could also deepen the understanding of the behaviour of individual columns. Finally, the test data could be further used to validate the numerical model which can be utilised to extend the parameters in tests and partially replace the costly fire tests [4].

This paper focuses on the study of temperature development of the composite joints; the structural behaviour will be published elsewhere. First, the test programme is introduced in detail. The tests considered two types of failure, i.e., failure during fire exposure (A'B' in Fig.1) and failure during loading after cooling down (D'E' in Fig.1). The effect of cooling phase was considered because the mechanical performance of the joints is likely to continue deteriorating in the cooling down phase

4

due to the high thermal inertia of concrete [4]. Another reason for considering the cooling phase is that an internal tensile force could develop in a restrained beam during the cooling phase, which may cause tensile failure in the joints. Secondly, experimental observation is reported, including (thermally-induced) failure modes and temperature-time relationships. The thermal behaviour of the joints is compared with individual columns. Thirdly, a finite element analysis (FEA) model is established and calibrated against the test data. The model is then employed to deepen the understanding of the temperature development and to eliminate the uncertainties in temperature measurement.

2. Experimental programme

The experimental programme of the composite joints followed up the previous experimental study of concrete-encased CFST columns [1]. The design for the column in the joint specimens was consistent with the column specimens. Besides, it also took into consideration the loading capacity of the facilities, the construction practice and the design codes.

2.1. Specimen preparations

In all, 10 double-sided cruciform specimens were designed and fabricated, as listed in Table 1. Two test types were designed, i.e., fire resistance test, denoted by R, and post-fire test, denoted by P. Test parameters included beam-to-column stiffness, load applied to the column, N_f, load applied to the beam, P_f, and duration of fire exposure, t_h. The beam-to-column stiffness was altered by changing the beam height. For specimens in groups J0 and J1, the beam heights were 300 mm and 350 mm, respectively. The load levels were determined according to the design codes and the test facilities. The heating time for post-fire tests were determined by multiplying the heating time ratio, t_o, and the fire resistance, t_R, which was obtained from the corresponding fire resistance test.

The specimens comprised one concrete-encased CFST column and two cantilever RC beams, as

shown in Fig.2a. Fig.2b shows the downward cross-section view of slicing the beam along cutting lines A-A (Fig.2a). Due to symmetry, the left half of A-A slices the beam at 20 mm depth and the right half cuts it at the mid-height. The steel tube and the longitudinal reinforcement in the column were continuous across the joint. The stirrups in the column were of 8 mm in diameter and arranged at spacing of 100 mm. To avoid localized failure of the concrete at both ends, two steel end collars of 100 mm in height were used. In the joint zone, to ensure the transmission of the shear force from the beam to the column, two stiffening steel sections were welded to the steel tube. The width of the RC beam was 200 mm at the cantilever ends; but increased to 300 mm (equal to the width of the column) at the joint end so that there was enough spacing in the outer concrete to accommodate the beam longitudinal reinforcement (Fig.2b). The top and bottom reinforcement in the beam was continuous across the joint zone. A 100-mm-depth RC slab was included at the top of the beam. A layer of reinforcing mesh with aperture size of 150 mm was used in slab (Fig.2b). Vent holes 1 and 4 (semicircle, Fig.2a) were pre-drilled at the workshop, whereas vent holes 2 and 3 (circle) were drilled just before tests. The latter two holes were drilled through the thickness of the steel tube to expose the concrete core. The benefit of drilling these two additional vent holes is that they could minimize the possibility of explosive fracture in the steel tube. This undesirable failure mode was observed in a parallel experimental study on concrete-filled steel tubular structures [25]. These vent holes were 20 mm in diameter.

The specimens were fabricated on the principle that uneven mass distribution and geometrical imperfections shall be minimized. In the workshop, inlet holes were pre-drilled in the top end plate (Fig.3a) and subsequently the end plates and stiffening steel sections were welded to the steel tube (Fig.2a). After fabrication, the assemblies were shipped to the yard outside the laboratory to construct the formwork. It is noteworthy that the longitudinal reinforcement in the column was tack-welded to

6

the bottom and the top end plates (Fig.3c). The specimens were kept in an upright position when casting the infilled concrete and the outer concrete. Prior to tests, the chamfered circular steel plates (Fig.3b and d) were welded back to the top end plate.

2.2. Material properties

To achieve exceptional seismic performance in practice, the load level of the inner CFST component shall be greater than the outer RC component. This is achieved by using concrete of a higher strength class for the core and loading the inner CFST component before the construction of the outer components. Considering this practice and the capacity of the test rig, the strength classes of the outer concrete and the infilled concrete were designed to be C25/30 and C40/50, respectively. Two batches of commercial concrete were ordered. For the concrete core, normal concrete with coarse siliceous aggregates was used. For the outer concrete, given the limited spacing of the reinforcement, concrete with siliceous-based fine aggregates (sizes 5-16 mm) was used to ensure consolidation. The mix ratio by weight for the outer concrete was: 1 cement: 0.73 water: 2.93 sand: 4.04 gravel: 0.37 admixture. The mix ratio for the inner concrete was not obtained from the supplier. The outer concrete was cast 42 days after that of the inner concrete. Specimen J0-1 was taken as a pilot test and tested when the infilled concrete had been cured for 350 days. The other specimens were tested at curing days of 552 to 591 days (for the infilled concrete). The concrete strength was obtained from standard test using $150 \times 150 \times 150$ mm cubes. For each batch of test, at least 3 samples were tested. Table 2 shows the measured cube strength of concrete at 28 days and test days.

The moisture content of concrete was measured by drying at 105°C in a ventilated oven for 24 h. Crushed concrete debris produced from the above strength tests was used as samples. To identify the effect of size, debris of various weights was selected. Prior to tests, loose bits on surface were brushed off. In all, three batches of tests were conducted at different curing days. The latter two

batches, containing 8 and 10 samples respectively, were conducted at the time of tests. The mean value of moisture content, *u*, at the time of test were measured to be 5.07% and 4.58% for the infilled concrete and the outer concrete, respectively. The corresponding standard deviations were 0.70% and 0.77%. Note that these values might not reflect the actual moisture contents as they were not obtained from standard specimens and the curing conditions could be different from the concrete in the specimens.

Steel coupons/bars were machined to obtain the mechanical properties of steel. The modulus of elasticity and Poisson's ratio were measured using strain gauges adhered on both sides of the samples. Table 3 lists the measured mechanical properties of steel.

2.3. Test setup and boundary conditions

The experiment was performed at the State Key Laboratory of Subtropical Building Science in South China University of Technology. The furnace had internal dimensions of 2.5×2.5×3 m and was equipped with 30 burners positioned at different heights (Fig.4b). The furnace temperature was controlled to follow the ISO-834 [26] standard temperature-time curve by a closed-loop control programme using furnace temperature and furnace pressure as inputs. Other details of the test setup are documented in [1].

The cantilever beams were free of constraint. The column nominally featured fixed-fixed boundaries. For the top end, the fixed boundary was achieved by (1) connecting the top end plate to a steel block using 12 high-strength bolts; and (2) constraining the motion of the steel block through four corner cylinders (Fig.4c), which were fixed to the reaction frame. During the fire exposure and the subsequent cooling down phase, the loads applied to both the column and the beam ends were kept constant by manually adjusting the actuator (for column) and jacks (for beams), i.e., allowing the column to elongate/shorten and the beams to bend.

2.4. Measurements

Although the column nominally featured fixed-fixed end conditions (Fig.4c and d), finite rotation of the top end inevitably occurred during tests due to the gap at the interfaces between the steel block and the cylinders (Fig.4c). To quantify this rotation, four LVDTs were arranged onto the top face of the steel block and thereby the rotation of the top end can be calculated using small rotation theory. The deflection of beams was measured by LVDTs which were positioned at 100 mm away from the cantilever end (Fig.4a). The deformation that occurred inside the furnace was not measured due to the limitation of the facilities.

The furnace temperature was monitored by 10 furnace thermocouples (Fig.4b); four threaded through the holes on the east side and two on each of the other sides. The furnace pressure was measured with a pressure sensor mounted on the east furnace wall.

K-type thermocouples, embedded in the concrete, were used to measure the internal temperature of the specimens. These thermocouples were 3 m in length and 6 mm in wire diameter. For both the column and the beams, two cross-sections were equipped with thermocouples. One cross-section was located outside the joint zone (Fig.5a and c) and the other within the joint zone (Fig.5b and d). Label BN2 denotes the thermocouple located within cross-section BN and numbered 2. The remainder of this subsection details the fixing methods and the positions of the thermocouples.

The main challenge for mounting thermocouples was how to fix them in the desired position to resist the vibration during concrete pouring. For the thermocouples located within the steel tube (CN4-6 and CJ3-5), a steel rod was employed as a support (Fig.5a and b). Prior to mounting into position, these thermocouples were fastened onto this rod. This assembly was subsequently threaded through the pre-drilled holes in the tube and then tack-welded to it. For the thermocouples located on the outer face of tube (CN3, CN7, CJ2 and CJ6), the wires were bent and tied onto the reinforcement.

Nevertheless, these tips could be disturbed during concrete casting. CN2 and CJ1 were fastened with tying wires onto the stirrups. CN8 and CJ7 were arranged longitudinally and tied to the longitudinal rebars. CN1 was used to measure the temperature of the fire-exposed concrete surface. The wires of thermocouple CN1 were cast in concrete and emerged from the opposite side. To ensure the tips of CN1 be exposed after demoulding, the thermocouples were held tight onto the inner face of the plywood. Nevertheless, the measuring tips of CN1 were more prone to being disturbed, which was inferred from the recorded temperature (Section 3.2).

For thermocouples BN(J)1, BN(J)3 and BN(J)4, the measuring tips and the wires were tied along the longitudinal rebars using normal tying wires (Fig.5c and d). For thermocouples BN(J)2, the wires were bent to form two spatial angles and then tied to the beam reinforcement. Their ends cantilevered out and the measuring tips were located at the centre of the cross-sections before casting concrete. The other end of the wires was arranged along the longitudinal rebars and emerged from the sides of specimens (Fig.4b). Since the thermocouples featured a smooth metal sheath and it is expected they would not affect the mechanical behaviour significantly.

The temperatures was recorded at time intervals of 1 min. For the post-fire tests, the recording of the temperature was terminated after the mean furnace temperature dropped below 100°C.

2.5. Test procedure and implementation

Two types of tests were performed, which were fire resistance tests (failure occurred under fire exposure) and post-fire tests (loaded to failure at ambient temperature after exposure to fire). The purposes of conducting the fire resistance tests were: (1) to study the behaviour of the composite joints in the fire situation; and (2) to obtain the fire limit which was used to determine the duration of fire exposure for the post-fire tests. The fire resistance tests included two phases (Fig.1), i.e., an initial phase for applying load at ambient temperature, AA', and a standard fire exposure phase, A'B'.

The loads were first applied to the column and then to the beams due to the difference in load level. These loads were applied at least 15 min before the commencement of fire tests. The failure criteria for axially loaded members and bending members in ISO 834-1 [27] were used for the column and the beams, respectively. The joints were deemed to have failed when either the beam or the column failed.

For the post-fire tests, the duration of fire exposure, t_h, was determined by multiplying the measured fire resistance, t_R, obtained from fire resistance tests, with the desired heating time ratio, t_o. Besides the two phases mentioned above, the post-fire tests contained two additional phases (Fig.1), i.e., a subsequent cooling down phase, B'C'D', and a post-fire loading phase, D'E'. Although a linear descending stage of θ-t relationship is prescribed by ISO-834 [26], the actual descending stage featured a decreasing cooling rate due to the limitation of the control system. In the post-fire phase, the loads on both beams were increased simultaneously until failure occurred. The maximum load attained was recorded.

The lower half of the joints was exposed to fire exposure; the exposed faces included the bottom face of the slab, three sides of the beam and four sides of the lower column (Fig.4b). Note that a 380 mm length at each end of the column projected out of the furnace and was covered by insulation. Ceramic fibre blanket of approximately 30 mm in thickness was glued on the unexposed surfaces using high-temperature adhesive. The thermal properties of ceramic fibre blanket provided by the manufacturer were the same with [18]: density at ambient temperature, 128 kg/m^3, and thermal conductivities 0.090, 0.176 and 0.220 W/(m·K) at 400 °C, 800 °C and 1000 °C, respectively. However, the data of specific heat was not available. For numerical purposes, the specific heat was assumed to be 1130 J/(kg·°C) according to the technical data of a similar product [28]. The thermal effect of the ceramic fibre blanket will be evaluated in Section 4.3.

3. Experimental results

This section presents and discusses the experimental findings. This first subsection concerns the fire-induced failure modes. The following subsections discuss the temperature of furnace, columns, beams and joints.

3.1. Failure mode

Beam failure was observed for all the tests (Table 1). Fig.6a and b show the views of specimen J1-2 during mounting and after test respectively. For the outer concrete in column, no fire-induced explosive spalling was observed mainly due to its low strength. For the beam, the corner concrete in the compression zone near the fixed end spalled. For the concrete core, there was no sign of explosive spalling. Major cracks formed on the top face of the slabs, whilst for the bottom face no crack was observed (Fig.6b). Fire-induced minute cracks on the column faces were observed.

The exposed surfaces of the lower column and beam turned whitish grey, while the upper face of the slab showed grey pink (Fig.6b). For concrete containing siliceous aggregate, the discolouration with respect to the exposed temperature is available in document [29]. Concrete colour remains normal when subjected to temperature up to 300 °C and turns pink if subjected to a temperature of 300 to 600 °C. This pink colour is due to the presence of ferrous salts. The pink discolouration suggested that the upper face of the slab could be subjected to a maximum temperature in the range of 300 to 600 °C. For the upper column, the colour change was insignificant, suggesting a maximum exposed temperature of below 300 °C. Note this observation of colour change could be subjective and the pink discolouration tends to be more prominent with siliceous aggregate [29]. Distinct gradients in colour change at the bottom of the upper column were observed.

After fire exposure, traces of water on the regions below the vent holes were noticed (Fig.6b). This suggested that the vent holes significantly contributed to the release of moisture during fire exposure.

3.2. Furnace temperature

The measured furnace temperature (θ) versus time (t) relationships, along with the average values (labelled AVE) are shown in Fig.7, taking specimens J0-1 and J0-4 as examples. The standard fire curve is also superimposed for comparison purpose. For J0-1 (Fig.7a), although the $\theta_{f,ave}$-value deviated from the standard curve during the first 5 min, it followed the ISO-834 standard curve reasonably well after this initial stage. The difference at 113 min was 4.2°C (0.41%). For J0-4 (Fig.7b), however, the average reading deviated from the standard curve by a greater extent. For instance, the average temperature deviated from the standard fire by 60 °C at 78 min, mainly because the control system failed to ignite additional burners. Comparing the readings of each thermocouple (inserted figures in Fig.7), there seems to be no consistency among different tests, indicating that this discrepancy was less likely to be caused by systematic error. For the other specimens, the average furnace temperature-time relationships are given in Figs.8 and 9.

3.3. Column temperature

The column temperature (cross-section CN, Fig.5a) shows the following characteristics:

(1) The θ–t curves exhibit a rapid increase during the first 10 to 20 min of heating, presumably because of the inward migration of moisture. This increase is prominent for thermocouples attached to the steel tube (CN3,4,6 and 7), and more pronounced for the thermocouples outside the steel tube (CN3 and 7) than those inside (CN 4 and 6). For example, CN7 increased by 56 °C from 11 to 14 min in J0-1 (Fig.8a). For J1-2, CN7 increased by 51 °C from 22 to 27 min (Fig.9b). Pure thermal conduction within concrete is unlikely to produce such a rapid temperature rise, as will be shown in Section 4.2. This effect was probably caused by the inward migration of moisture, as previously observed in RC columns by Lie and Irwin [30]. They pointed out that this effect was observed in a depth range of 64 to 152 mm (centre of their specimens).

By comparison, although the concrete-encased CFST columns herein are of similar cross-sectional dimensions, this effect seemed to be observed at a depth of 70 mm only. At a depth of 150 mm (centre, CN5), however, the temperature rise was relatively gradual. Such a difference suggested that the steel tube might prevent moisture from migrating inwards, and thus delayed the temperature rise of the concrete core.

(2) The θ–t curves of thermocouples attached to the steel tube exhibited a pronounced moisture plateau at approximately 100 °C. For J0-1, CN7 and CN3 exhibited plateaus lasting about 34 and 37 min respectively (Fig.8a). For J0-4, the plateaus of CN3 and CN7 lasted about 30 and 20 min respectively (Fig.8d).

To quantitatively compare the duration of the moisture plateau, the statistical values for each thermocouple are graphed in a box chart (Fig.10). The duration is defined as the time during which the temperature increases from 100 to 120 °C. Of thermocouples labelled CN, CN3 and CN7 exhibited the longest moisture plateaus. Considering that this characteristic is not pronounced for conventional CFST columns [31][32], it is inferred that it might be caused by two factors. First, the migration of moisture at the initial stage of fire exposure accelerated the temperature rise of the inner components, as mentioned above. Secondly, the presence of the steel tube and outer component (about 70 mm in thickness) might impede the heated moisture moving inwards.

The effects of these interacting factors could be complex. On one hand, the delay of the temperature rise near the steel tube can be beneficial in terms of fire resistance. On the other hand, it can also be detrimental because the build-up of the pressure may cause explosive fracture in the steel tube, as previously observed in [25]. It also suggests that the effectiveness of vent holes shall be ensured for concrete-encased CFST structures.

(3) The temperature of the steel tube (approximated using the mean value of the inner and outer face

temperatures) ranged from 271 to 507°C when the specimens failed in the fire situation. Previous study of individual concrete-encased CFST columns have found that the critical temperature of steel tube ranges from 401 to 698°C [1]. This difference is reasonable because the failure of the joint specimens was governed by the RC beams. For the post-fire tests, the maximum temperature attained during the heating and cooling phases (θ_{max}) ranged from 177 to 276 °C. The critical temperature and θ_{max} confirmed the passive protection provided by the outer RC component.

(4) Corner concrete was more vulnerable to fire exposure after 30 min, which is consistent with the literature review conducted by Hertz [33]. For the fire resistance tests, although CN8 started at a lower temperature at the onset of fire tests, it increased considerably from 30 to 40 min and exceeded that of CN2 (e.g. at 78 min for J0-2, Fig.8b). This is expected, because the corner concrete was exposed to fire on two sides. The numerical study in Section 4.2 also confirms this. Considering that concrete explosive spalling was not pronounced (Fig.6b), the formation of thermally-induced minute cracks at the corner might give a plausible explanation.

Interestingly, the temperature of CN8 exceeded CN1 in a later stage (e.g. at 90 min for J0-5, Fig.8e). This suggests possible displacement of the tips of CN1 during concrete pouring.

(5) The temperature difference between thermocouples CN4 (or CN6) and CN3 (or CN7) could not be deemed as the temperature difference between the inner face and outer face of the steel tube. The difference recorded in tests was significant probably because: (1) there could be concrete in between the tip of thermocouple and the face of steel tube (e.g., CN3 and CN7, Fig.5a); and (2) the tips could be displaced during concrete pouring. The numerical simulation (Section 4.2) suggests the difference between the inner face and outer face is limited due to the high thermal conductivity of steel.

(6) For the concrete core (CN5), the θ-t curves exhibit a plateau at a temperature significantly higher than 100 °C. For J0-5 (Fig.8e), a plateau spanning from 130 to 150 min is observed; similar plateaus

also appear at 130 min for J1-1 (Fig.9a) and 160 min for J1-2 (Fig.9b). These plateaus are observed for CN5 (centre) only, which suggests that it was possibly caused by local thermo-mechanical behaviour of moisture [33] or chemical behaviour of concrete [34].

3.4. Beam temperature

(1) The highest temperature was recorded by BN1, e.g., 987°C for J0-6 (Fig.8f). The shallow depth of BN1 (30 mm) made it less susceptible to moisture effect; the decrease of the rate of temperature rise at about 10 to 15 min (Fig.8a) was limited.

(2) The temperature of BN2 and BN3 increased much slower and were affected by moisture to a greater extent. The plateau lasts for up to 38 min for BN3 (J0-5, Fig.8e). This extended plateau might result from three factors: (1) these depths were subjected to a relatively lower heating rate; (2) the rapid initial temperature rise due to the migration of moisture from shallower depths; and (3) the difficulty of moisture to migrate to the outside. For the second factor, the highest rate of temperature rise was about 28.8 °C/min attained at 20 min (J0-5, Fig.8e). The migration of moisture brought forward the time when the temperature reached 100 °C, as will be shown in Section 4.3.

(3) The θ-t curves of BN4 show an increased rate in temperature rise at 50 to 60 min for specimens J0-5, J0-6 and J1-3 (Fig.8e, f and Fig.9c). Given that the ceramic fibre blanket used at the upper face of the slab was about 30 mm, it is possible that the blanket lost its effectiveness of thermal insulation. This effect will be studied using the numerical method (Section 4.3).

3.5. Joint temperature

(1) Compared with the temperatures of CN, the temperatures of CJ were tremendously reduced due to the combined effect of heat sink and the passive protection of the outer concrete encasement. For specimens with $t_R \leq 150$ min (J0-1, J0-2 and J1-1), the joint temperature (thermocouples labelled CJ) did not exceed 150°C when fire limit was reached. For the specimens with $t_R > 200$ min (J0-5, J0-6,

J1-2 and J1-3), the temperatures of joint were below 300°C at fire limit.

(2) The temperatures of BJ, however, were influenced by the heat sink effect to a lesser extent in the early stage of fire exposure. This is expected, because cross-section BJ was positioned 100 mm away from the column edge. It is noticed that the heat sink effect became obvious in the late stage of fire exposure. For example, the θ–t curves of BN1 and BJ1 (J0-5, Fig.8e) overlap each other throughout the initial 60 min, but BN1 exceeded that of BJ1 afterwards. Likewise, for post-fire test J0-6 (Fig.8f), the temperature of BJ1 became lower than BN1 only after 40 min of fire exposure. This shows that the heat sink effect was limited to the joint zone in the early stage of fire exposure, but spread gradually in a later stage. This is possibly because in the late stage the heat transferred to the colder upper column faster due to the greater temperature gradient in the joint zone.

(3) Fig.10 shows that the duration of plateaus of the joint zone exceeded that of the non-joint zone significantly. This indicates the configuration of the joint effectively delay the heat transfer from the hot members to the colder connected member. Note that such a long duration of the plateau was not purely due to the effect of moisture; the low thermal conductivity of concrete in nature gave rise to the slow heating as well.

3.6. Effect of test parameters on temperature

To study the effect of beam height on temperature, the temperatures attained at 200 min were extracted from specimens J0-5, J0-6, J1-2 and J1-3 (Fig. 11). It shows that the temperature difference is insignificant, especially for the joint zone. This seems to be reasonable because increasing beam height increases the distance for the heat transferred from the bottom surface only; but not affects the heat transferred from beam sides.

Load level does not seem to have a noticeable effect on temperature either. But it is noticed that specimens with a higher beam load level tended to exhibit a slightly severer spalling in the

compression zone of the fixed end of the beam.

4. Numerical study

A numerical study was conducted to complement the experiments. This section introduces the establishment of the FEA model and validations. The purposes of the numerical modelling are: (1) to eliminate uncertainties in the interpretation of the test results; (2) to further understand the temperature developments of the joints; and (3) to prepare for future numerical modelling of the structural behaviour.

4.1. Establishment of the FEA model

Considering that cross-sections CN and BN were not subjected to the heat sink effect, their temperatures were used to calibrate the heat transfer model in a first step. To benefit from computational efficiency and accuracy, two-dimensional (2D) FEA models (Fig.12) were established for this purpose. The 2D models are advantageous also because a finer mesh can be used for the cross-sections, whereas the three-dimensional (3D) model (Fig.13), especially the sequentially coupled thermal-stress analysis models, have to use a relatively coarse mesh to achieve computational efficiency. The 2D models were also used to examine uncertainties, including the displacement of the measuring tips, the thickness and specific heat of the ceramic fibre blanket. In a second step, three-dimensional (3D) FEA heat transfer analysis models (Fig.13) were employed to further validate the 2D models and to study the temperatures of cross-sections CJ and BJ.

4.2. Predicted temperature of cross-section CN

One quarter of cross-section CN was modelled (Fig.12a). Four-node linear heat transfer elements (labelled DC2D4 in Abaqus element library [35]) were used for the concrete, steel tube and longitudinal reinforcement. For simplicity, stirrups were ignored in this 2D model. The dimensions of elements ranged from 2.5 to 8 mm, and the maximum aspect ratio was less than 2.6. Note that the mesh

at the regions near the thermocouples was refined for the purpose of examining the effect of possible erroneous measurement. The measured average furnace temperature-time curves were input to define the thermal boundary condition. For the fire-exposed surfaces, the thermal emissivity coefficient was taken as 0.7 and the coefficient of heat transfer by convection was 25 W/m^2·K according to Eurocode 4 [36] and Eurocode 1 [37] respectively. For the unexposed surfaces (right and bottom in Fig.12a), no thermal boundary was applied. The steel-concrete interfaces were modelled using the 'tie' constraint, neglecting the thermal effect of the air-gaps at these interfaces. Note that this assumption could give rise to a higher temperature prediction. The previous study [2] examined the effect of the thermal conductance at the steel-concrete interface. Its results show that introducing the thermal conductance has a limited effect on the temperature of the outer concrete, but reduces the temperature of the concrete core.

The thermal properties of materials proposed by Lie [38] and Eurocode 4 [36] were both employed. When using Lie's model, the effect of moisture was modelled by using an equivalent specific heat for concrete for temperature below 100°C, which is given in [16]. Two values of moisture contents, i.e., u=5%, 8%, were used for the concrete core in the models. Note that u=8% was extremely unlikely to occur for the tests herein; the possible maximum moisture content can be calculated from the mix ratio. For the outer concrete, the maximum possible moisture was 8.08%. For the infilled concrete whose strength was higher (the corresponding water-to-cement ratio was lower), the maximum possible moisture could be even lower. The results are given for comparison purpose only. In this stage, individual predicted temperatures were compared with the measured values. For the fire resistance tests, the temperature attained at fire limit was extracted, whereas for the post-fire tests the maximum temperature attained during the full-range fire (θ_{max}) was obtained.

Fig.14 compares the predicted temperatures with the measured ones. Lie's thermal properties

overestimated the temperatures of CN; 25 out of 74 predictions lies outside ±20% limits (Fig.14a). Most outliers are from CN4 to 6 (inside the steel tube). Note that the predicted temperatures for CN3, CN4, CN7 and CN8 came from a depth of 3 mm (wire radius) in the concrete (as shown in Fig.5a and Fig.12a), rather than the ideal steel-concrete interface. This is to consider the possible effect of erroneous measurement. These deviations in Fig.14a were probably because the thermal properties could not reflect the significant effect of moisture on the temperature development of the concrete core. Likewise, the corresponding predicted values of CN1 were extracted from the 6-mm depth beneath the concrete surface (Fig.12a), assuming a situation where the measuring tips displaced by 6 mm (diameter). Nevertheless, the predicted temperatures for some specimens still exceeded the test results, such as J0-3 (Fig.14a). This is possibly because the measuring tip was significantly disturbed; thus pursuing better agreement for these cases might be meaningless.

Fig.14b compares the measured temperature with the predicted temperature when the thermal properties given in Eurocode 4 were used and a moisture content of 5% was assumed for the infilled concrete. The corresponding mean value of θ_c/θ_e, standard deviation (SD) and coefficient of variation (COV) are tabulated in Fig.14b. There data show that moisture content had a minor effect on the overall predicted temperatures. Fig.14b shows that most of the values are within ±20% error. The outliers are from CN1 and CN5. Compared with Fig.14a, it can be found that the prediction for CN1 of specimens J0-3 have not been improved significantly, which seems to confirm the unreliable temperature measurement for CN1. By contrast, the predictions for CN4 and CN6 (outliers in Fig.14a) have been improved considerably, demonstrating the thermal properties in Eurocode 4 could better address the effects of moisture on the temperature of the concrete core.

4.3. Predicted temperature of cross-section BN

The thermal properties given by Eurocode 4 were used for modelling the temperatures of

cross-section BN. As aforementioned, the specific heat and thickness of ceramic fibre blanket are the two main sources of uncertainty. During mounting, the blanket could be easily compacted; therefore, it was difficult to measure the true thickness. In the simulation herein, the specific heat was assumed to be fixed at 1130 J/(kg·°C). Meanwhile, a series of thicknesses, ranging from 15 to 35 mm, were explored.

Fig.15 compares the measured temperatures and the predicted temperatures for the case where the thickness of ceramic fibre blanket, a, was assumed to be 25 mm. The mean value of θ_c/θ_e, standard deviation (SD), and coefficient of variation (COV) for other thicknesses are also tabulated in Fig.15. In terms of the mean θ_c/θ_e–values, the thickness of 25 mm gave the most accurate predictions. In all, 5 of 40 values lie out of the ±10% limits. The outlier of BJ2 of specimen J1-3 shows a major deviation. Considering that the predicted temperature for BJ2 of duplicate specimen J1-2 shows a good agreement with the measured value, the deviation is probably resulted from erroneous measurement due to the displacement of the measuring tip. Fig.15 suggests that if the specific heat of the ceramic fibre blanket is assumed to be 1130 J/(kg·°C), then a thickness of 25 mm seems to produce the most satisfactory predictions for the temperatures of cross-section BN.

4.4. Comparison between the predictions of 2D and 3D models

The 3D FEA model was used to generate the temperature distribution of the joints. It is essential to verify that the 2D and 3D FEA models generate consistent results and also the comparison would eliminate any possible error in modelling. In this respect, the temperatures of cross-sections BN and CN obtained from the two FEA models are compared, as shown in Fig.16. Note that in the FEA models temperatures from the identical geometrical points, i.e., neglecting the possible displacement of the measuring tips, are compared. Fig.16 shows that the predicted temperatures of the two FEA models are in good agreement. The outliers for CN5 and BN3 were possibly due to the differences in

meshing.

4.5. Temperature-time relationships

The measured and predicted temperature (θ) versus time (t) relationships are shown in Figs.17 and 18, taking specimens J0-5 (fire resistance test) and J0-4 (post-fire test) as examples because they were subjected to longer fire exposure. For clarity, the θ–t curves for each specimen was presented in two subfigures. The temperatures of cross-sections BN and CN came from the 2D FEA model since it provided a finer mesh, while the temperatures of cross-sections BJ and CJ came from the 3D model. The remainder of this subsection focuses on the comparison of the θ–t curves.

As shown in Fig.17a, the increasing deviation between the predicted and measured temperature for CN1 indicates that the measured values might come from a depth of greater than 3 mm beneath the concrete surface. For CN2, CN4 and CN6, the FEA model overpredicted the temperature. Nevertheless, the difference between the predicted and measured temperatures were relatively constant after 150 min. The comparison of CN4 and CN6 confirms that the lower increasing rate of the measured temperature after 100 min was possibly due to the local thermal effect that could not be reproduced by the models. For CN5, the predicted temperature was about 90 °C lower than the measured temperature at 120 min, but it increased and exceeded the measured temperature at around 170 min. This difference possibly results from the assumption that the peak value of the specific heat of concrete incorporating the moisture effect situated at 115 °C in the modelling [36]. It is possible that the temperature could be influenced by the moisture at a temperature range higher than 115 °C due to the build-up of the inner pressure. For CN7, the sharp rise at 53 min is not reproduced by the numerical model. However, the deviation gradually levelled off at a later stage. For CN8, a gradual increase of the difference at the late stage of fire exposure is noticed. This is probably caused by the formation of minute cracks at the corner.

For BN1, BN2 and BN3 (Fig.17a), acceptable agreements are reached between the predicted and measured θ–t curves; the former was about 50 °C higher than the latter at 224 min. For BN4, if adiabatic condition is assumed for the top face of the slab, then the predicted temperature (labelled BN4-1) is considerably lower than the measured one which shows a steeper increase after 40 min. The assumption of a thickness of 15 mm for the blanket improves the predictions (BN4-2); but overestimates the temperature. A thickness of 25 mm gives the most satisfactory predictions (BN4). This confirms that the ceramic fibre blanket shall be modelled to consider the heat transmitted from the top face of the slab.

For BJ1 (Fig.17b), the predicted and the measured θ–t curves are in good agreement. The deviation of BJ2 and BJ3 was caused by the effect of moisture, as indicated by the plateau at about 100 °C in θ–t curves. For BJ4, again, a thickness of 25 mm produces a good agreement. BJ4-1 and BJ4-2 denote the situations where adiabatic condition was used and where the thickness was assumed to be 15 mm respectively. The predicted temperatures are higher than the measured ones except for CJ4. This shows that the effect of moisture seems to be beneficial. Apart from CJ7, thermocouples CJ attained temperatures less than 300 °C.

The discussion related to post-fire tests (Fig.18) will pay more attention to the time when the maximum temperature was attained and the descending branch of θ–t curves. For θ_{max} exceeding 300 °C, e.g. BN1 and BJ4, the predicted time corresponding to θ_{max} agrees well with the test results. For θ_{max} below 300 °C, the time when θ_{max} was attained in prediction could either before the measured one, e.g. CN4 (Fig.18a) and BJ3 (Fig.18b), or after the it, e.g. CJ6 (Fig.18b), probably because of the effect of moisture. In terms of the descending branch of θ–t curves, the predicted ones show a sharper decreased, as opposed to the measured ones, e.g. CN1 (Fig.18a) and BJ1 (Fig.18b). This is mainly due to the assumption that the thermal properties of materials during cooling down were identical to that

under heating. An experiment study suggests that the thermal conductivity and specific heat of concrete at temperature range of 0 to 200 °C during the cooling phase can be lower than that in the heating phase [34]. It is possible to improve the temperature prediction for the cooling phase if experiment-based thermal properties for cooling phase are incorporated. But this requires more efforts and needs comprehensive test evidence because the thermal properties during the cooling down phase are dependent on a variety of factors. For the current study, it is deemed acceptable if a good agreement on the maximum temperature is obtained.

5. Conclusions

This study sets out to experimentally and numerically investigate the temperature development of a beam-to-column composite joint subjected to the full-range fire including heating and cooling phases. The test programme has been presented in detail. Experimental results related to temperature have been reported and further compared with the results of the numerical models. Within the limitation of this study, the following conclusions can be drawn:

(1) Beam failure was observed for all tested specimens. For the outer concrete in column, there was no sign of explosive spalling due to its low strength. Fire-induced minute cracks formed on the column surface. The measured temperature suggests that the formation of the minute cracks seemed to accelerate the temperature rise of the corner concrete. For the slab, the pink discolouration of the top face suggests that the slab was subjected to heat attack during tests.

(2) The temperature versus time curve exhibits a rapid increase in the early stage of fire exposure due to the inward migration of moisture. For the thermocouples attached to the steel tube, the temperature versus time curves exhibit a pronounced moisture plateau. At fire limit, the temperature of the steel tube was significantly lower than that in the individual column members in the previous study.

(3) The temperature versus time curve of the centroid of the beam cross-section and the upper half

could be affected by moisture to a greater extent. For the thermocouple in the concrete slab, the increased rate in temperature rise at 50 to 60 min reveals possible heat penetration into the fibre blanket. Beam height and load level did not show a significant effect on temperature.

(4) The temperature of the joint zone was tremendously reduced compared to the non-joint zone. The long duration of the plateau in temperature-time curves indicates that the configuration of the joints effectively delayed the heat transfer from the hot members to the colder connected member. The effect of heat sink was limited to the joint zone in the early stage of fire exposure, but spread gradually in a later stage, plausibly due to the increasing temperature gradient in the joint zone.

(5) The FEA model produced satisfactory temperature predictions if the thermal properties in Eurocode 4 was used. The deviation of the predication could be possibly caused by the displacement of the measuring tips of the thermocouples during concrete pouring. The parametric study on the thickness of the ceramic fibre blanket identified that the case in which the thickness was assumed to be 25 mm produced the most satisfactory predictions for beam temperature. The results of the 2D model and the 3D model were consistent.

(6) The FEA model herein was unable to encompass every factor. Factors such as the thermal conductance at the steel-concrete interface and the effect of cracks (or spalling) on temperature were not incorporated. Besides, in the absence of comprehensive test evidence for the thermal properties for the cooling phase, they were assumed to be identical with those for the heating phase. Addressing these factors could potentially further improve the temperature prediction.

Being limited to the thermal behaviour of the composite joints, this study does not report the experimental results related to structural behaviour and lacks the corresponding discussions. They will be reported and explored in further research.

Acknowledgements

Declarations of interest

None.

References

[1] Zhou K, Han L-H. Experimental performance of concrete-encased CFST columns subjected to full-range fire including heating and cooling. Engineering Structures. 2018;165:331-48. https://doi.org/10.1016/j.engstruct.2018.03.042.

[2] Zhou K, Han L-H. Modelling the behaviour of concrete-encased concrete-filled steel tube (CFST) columns subjected to full-range fire. Engineering Structures. 2019;183:265-80. https://doi.org/10.1016/j.engstruct.2018.12.100.

[3] Al-Jabri KS, Davison JB, Burgess IW. Performance of beam-to-column joints in fire—A review. Fire Safety Journal. 2008;43:50-62. https://doi.org/10.1016/j.firesaf.2007.01.002

[4] Lennon T, Moore DB, Wang YC, Bailey CG. Designers' Guide to EN 1991-1-2, 1992-1-2, 1993-1-2 and 1994-1-2 - Handbook for the Fire Design of Steel, Composite and Concrete Structures to the Eurocodes. ICE Publishing.

[5] Nethercot DA. Connection research and its impact on practice during the Dowling era. Journal of Constructional Steel Research. 2006;62:1165-70. https://doi.org/10.1016/j.jcsr.2006.06.008

[6] Wang YC, Davison JB, Burgess IW, Plank RJ, Yu HX, Dai X. The safety of common steel beam/column connections in fire. The Structural Engineer. 2010, 88(21): 26-35.

[7] Wang YC. Performance Based Fire Engineering Research of Steel and Composite Structures: A Review of Joint Behaviour. Advances in Structural Engineering. 2011;14:613-24. 10.1260/1369-4332.14.4.613

[8] Han L-H, Xu C-Y, Tao Z. Performance of concrete filled stainless steel tubular (CFSST) columns and joints: Summary of recent research. Journal of Constructional Steel Research.

2019;152:117-31. https://doi.org/10.1016/j.jcsr.2018.02.038

[9] Haremza C, Santiago A, Demonceau J-F, Jaspart J-P, da Silva LS. Composite joints under M-N at elevated temperatures. Journal of Constructional Steel Research. 2016;124:173-86. https://doi.org/10.1016/j.jcsr.2016.05.012

[10] Fischer EC, Selden KL, Varma AH. Experimental Evaluation of the Fire Performance of Simple Connections. Journal of Structural Engineering. 2017;143:04016181.doi:10.1061/(ASCE)ST.1943-541X.0001664

[11] Song T-Y, Han L-H, Uy B. Performance of CFST column to steel beam joints subjected to simulated fire including the cooling phase. Journal of Constructional Steel Research. 2010;66:591-604. https://doi.org/10.1016/j.jcsr.2009.12.006

[12] Tan Q-H, Han L-H, Yu H-X. Fire performance of concrete filled steel tubular (CFST) column to RC beam joints. Fire Safety Journal. 2012;51:68-84. https://doi.org/10.1016/j.firesaf.2012.03.002

[13] Song T-Y, Han L-H. Post-fire behaviour of concrete-filled steel tubular column to axially and rotationally restrained steel beam joint. Fire Safety Journal. 2014;69:147-63. https://doi.org/10.1016/j.firesaf.2014.05.023

[14] Pascual AM, Romero ML, Tizani W. Fire performance of blind-bolted connections to concrete filled tubular columns in tension. Engineering Structures. 2015;96:111-25. https://doi.org/10.1016/j.engstruct.2015.03.067

[15] Yang Y-F, Fu F. Fire resistance of steel beam to square CFST column composite joints using RC slabs: Experiments and numerical studies. Fire Safety Journal. 2019;104:90-108. https://doi.org/10.1016/j.firesaf.2019.01.009

[16] Song T-Y, Han L-H, Yu H-X. Temperature Field Analysis of SRC-Column to SRC-Beam Joints Subjected to Simulated Fire Including Cooling Phase. Advances in Structural Engineering. 2011;14:353-66.10.1260/1369-4332.14.3.353

[17] Song T-Y, Han L-H, Tao Z. Structural Behavior of SRC Beam-to-Column Joints Subjected to Simulated Fire Including Cooling Phase. Journal of Structural Engineering. 2015;141:04014234.doi:10.1061/(ASCE)ST.1943-541X.0001211

[18] Song T-Y, Tao Z, Razzazzadeh A, Han L-H, Zhou K. Fire performance of blind bolted composite beam to column joints. Journal of Constructional Steel Research. 2017;132:29-42. https://doi.org/10.1016/j.jcsr.2017.01.011

[19] Pucinotti R, Bursi OS, Demonceau JF. Post-earthquake fire and seismic performance of welded steel–concrete composite beam-to-column joints. Journal of Constructional Steel Research. 2011;67:1358-75. https://doi.org/10.1016/j.jcsr.2011.03.006

[20] Pucinotti R, Bursi OS, Franssen JM, Lennon T. Seismic-induced fire resistance of composite welded beam-to-column joints with concrete-filled tubes. Fire Safety Journal. 2011;46:335-47. https://doi.org/10.1016/j.firesaf.2011.05.003

[21] Raouffard MM, Nishiyama M. Fire response of exterior reinforced concrete beam-column subassemblages. Fire Safety Journal. 2017;91:498-505. https://doi.org/10.1016/j.firesaf.2017.03.054

[22] Liao F-Y, Han L-H, Tao Z. Behaviour of composite joints with concrete encased CFST columns under cyclic loading: Experiments. Engineering Structures. 2014;59:745-64. https://doi.org/10.1016/j.engstruct.2013.11.030

[23] Zhou X, Zhou Z, Gan D. Cyclic testing of square tubed-reinforced-concrete column to RC beam joints. Engineering Structures. 2018;176:439-54. https://doi.org/10.1016/j.engstruct.2018.09.053

[24] Ma D-Y, Han L-H, Zhao X-L. Seismic performance of the concrete-encased CFST column to RC beam joint: Experiment. Journal of Constructional Steel Research. 2019;154:134-48. https://doi.org/10.1016/j.jcsr.2018.11.030

[25] Han L-H, Song T-Y, Zhou K and Cui Z-Q. Fire Performance of CFST Triple-Limb Laced Columns. Journal of Structural Engineering, 2018, 144(9): 04018157. DOI:10.1061/(ASCE)ST.1943-541X.0002168.

[26] ISO-834. Fire-resistance tests - Elements of building construction. International Standard: Geneva; 1975.

[27] ISO-834-1. Fire-resistance tests-elements of building construction - Part 1: General requirements. International Standard ISO 834, Geneva; 1999.

[28] Morgan Advanced Materials. Product Data Book. Available at: http://www.morganthermalceramics.com/media/5454/morgan-advanced-materials_thermal-ceramics-product-data-book-e-version_2.pdf (accessed 21 May 2019).

[29] Concrete Society, Assessment and Repair of Fire-Damaged Concrete Structures. 1990. Technical Report No. 15, The Concrete Society, UK.

[30] Lie TT, Irwin RJ. Evaluation of fire resistance of reinforced concrete beam-columns with rectangular cross-section. Ottawa (Canada): NRC-CNRC Internal Report, No.601; 1990.

[31] Han L-H, Yang Y-F, Xu L. An experimental study and calculation on the fire resistance of concrete-filled SHS and RHS columns. Journal of Constructional Steel Research. 2003;59:427-52. https://doi.org/10.1016/S0143-974X(02)00041-X

[32] Lie TT, Chabot M. Experimental Studies on the Fire Resistance of Hollow Steel Columns Filled with Plain Concrete. Internal Report (National Research Council Canada Institute for Research in Construction); no IRC-IR-611: National Research Council Canada; 1992.10.4224/20358480

[33] Hertz KD. Limits of spalling of fire-exposed concrete. Fire Safety Journal. 2003;38:103-16. https://doi.org/10.1016/S0379-7112(02)00051-6

[34] Zehfuß J and Lyzwa J. Thermische Materialeigenschaften Von Beton In Der Abkühlphase, in Tagungsband of Braunschweiger Brandschutz-Tage 2017, September 13-14, 2017 Braunschweig, Germany. Zehfuß J, Eds. Braunschweig. (In German)

[35] Abaqus. Abaqus 2017 Documentation, Dassault Systèmes, Providence, RI, USA; 2017.

[36] CEN (European Committee for Standardization). Eurocode 4 - Design of composite steel and concrete structures; Part 1-2: General rules-Structural fire design. EN 1994-1-2:2005+A1:2014. Brussels, Belgium; 2014.

[37] CEN (European Committee for Standardization). Eurocode 1: Actions on structures–Part 1–2: General actions–actions on structures exposed to fire. EN 1991-1-2:2002. Brussels, Belgium; 2009.

[38] Lie TT. Fire resistance of circular steel columns filled with bar-reinforced concrete. Journal of Structural Engineering. 1994;120:1489-1509. doi:10.1061/(ASCE)0733-9445(1994)120:5(1489)

Captions for figures

Fig. 1. Complete temperature (θ)-load (N)-time (t) path.

(a) Elevation

(b) Cross section A-A

Fig. 2 Detailed design of the specimens (units in mm).
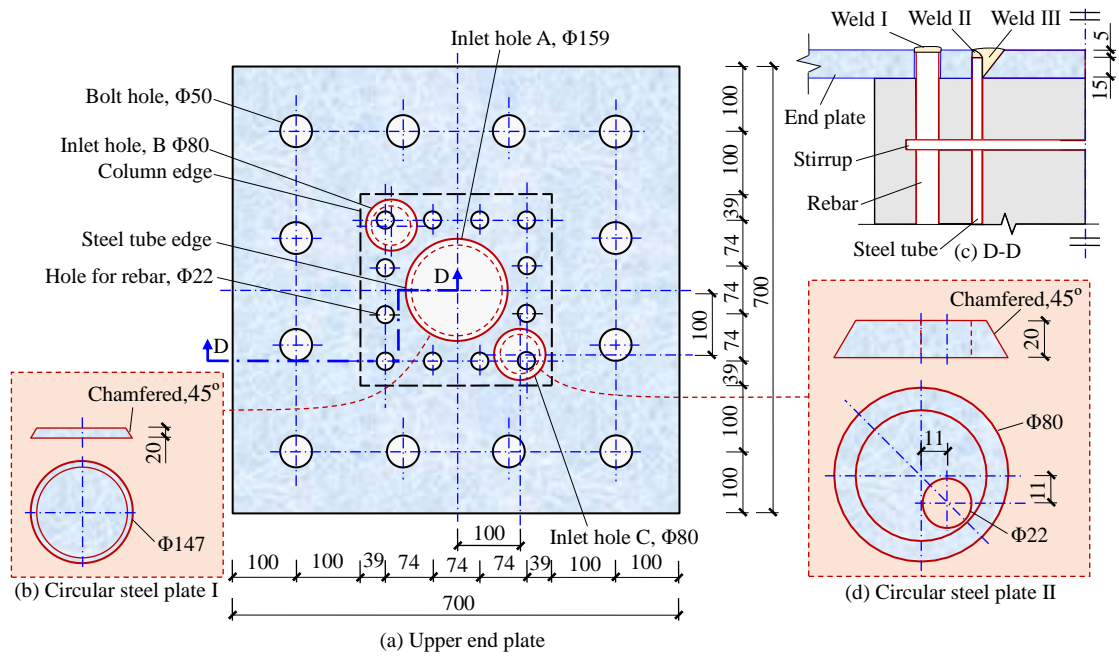
Fig. 3 Detailed design of the top end plate (units in mm).

| (a) Beam end | (b) Front view | (c) Top end |
| | | (d) Bottom end |

Fig. 4 Test setup.

CN8
CN7
CN6
Steel rod Φ6
CN5
CN4
CN3
CN2
CN1
Φ159
12Φ16
30
300
300

(a) Cross-section CN-CN

CJ7
CJ6
CJ5
Steel rod Φ6
Stiffening steel section
CJ4
CJ3
CJ2
CJ1
Φ159
Beam bottom rebar
12Φ16
Φ8@10
30
300
300
Beam edge
Column edge
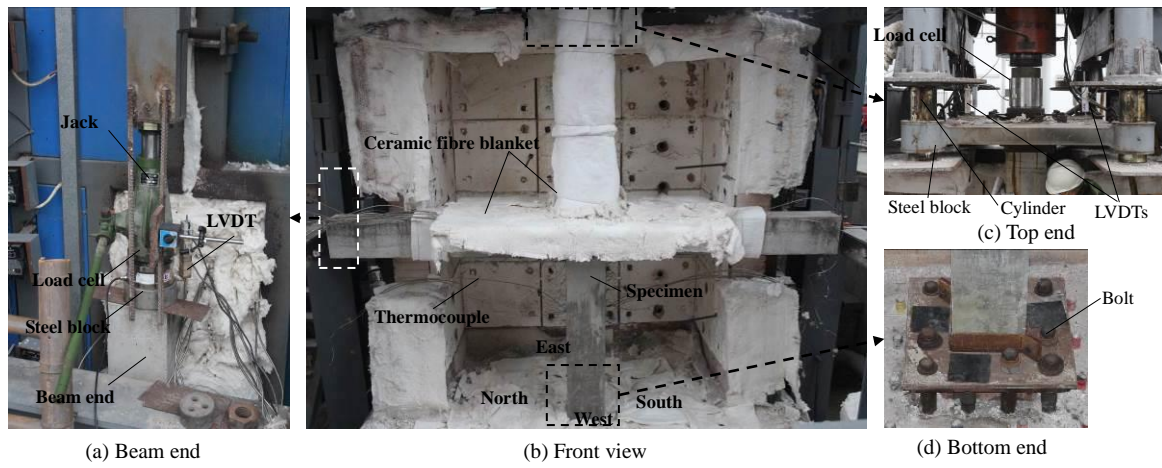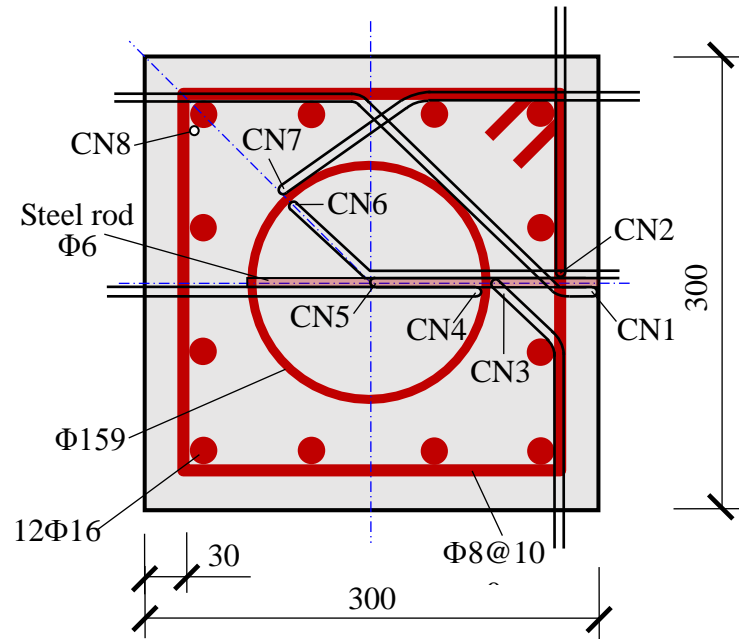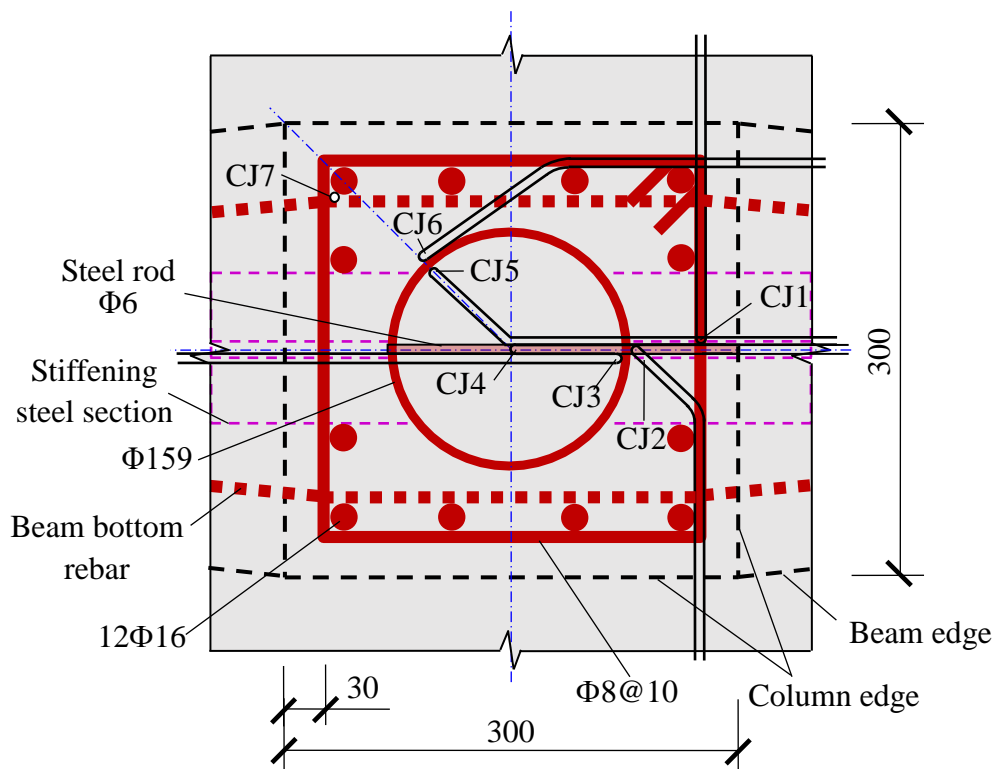
(b) Cross-section CJ-CJ

6
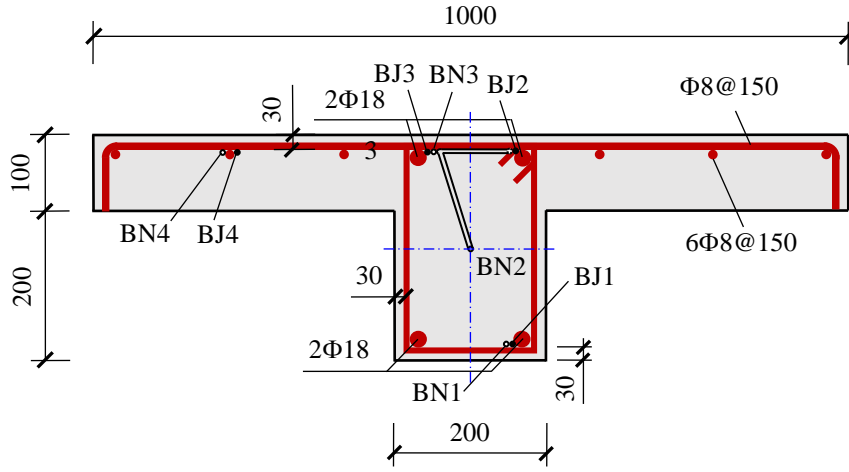
(c) Cross-section BN-BN for group J0
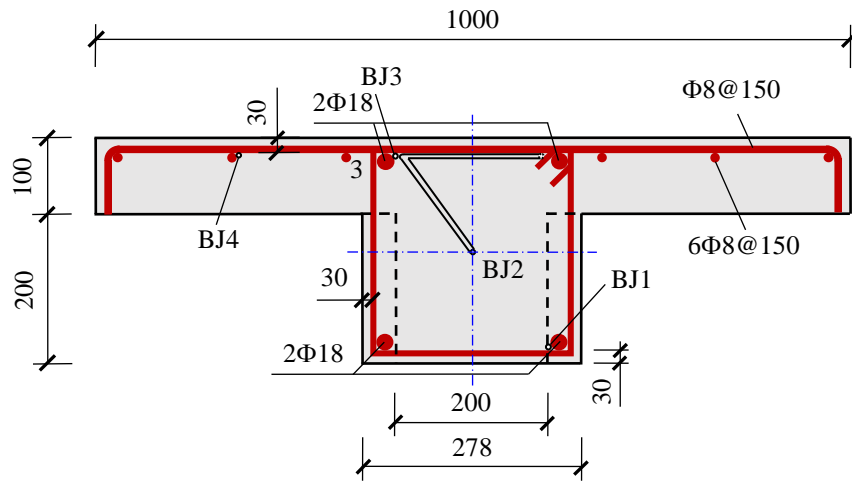
(d) Cross-section BJ-BJ for group J0

Fig. 5 Detailed arrangement of the thermocouples (units in mm).

Note. For thermocouples whose wires were arranged perpendicular to the cross-section, empty/solid dots are used. An empty dot denotes the tip is at this cross-section, e.g., BN4 in (c). A solid dot denotes the wire of the thermocouple intersects the cutting plane and the tip is in the joint zone, e.g., BJ4 in (c) and its tip is at cross-section BJ-BJ (d). For thermocouples whose wires were arranged within the cross-section, the wires are shown, e.g., CJ6 in (b).
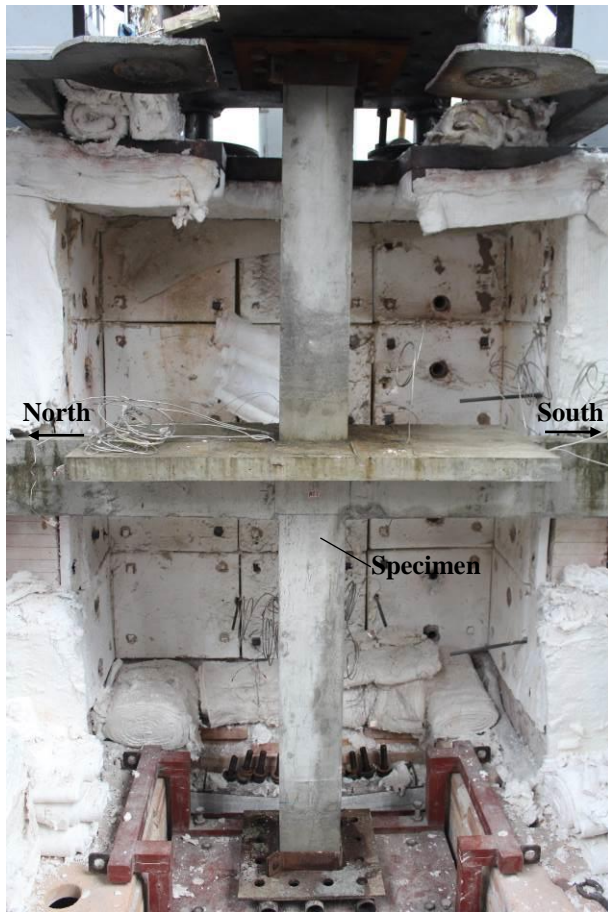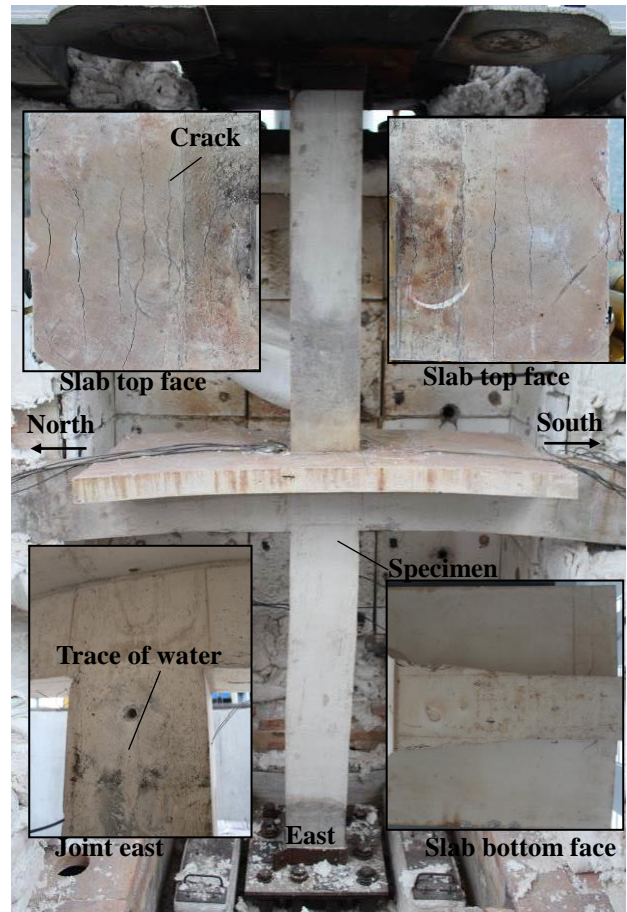
(a) During mounting   (b) After exposure to fire

Fig. 6 Failure modes (specimens J1-2).
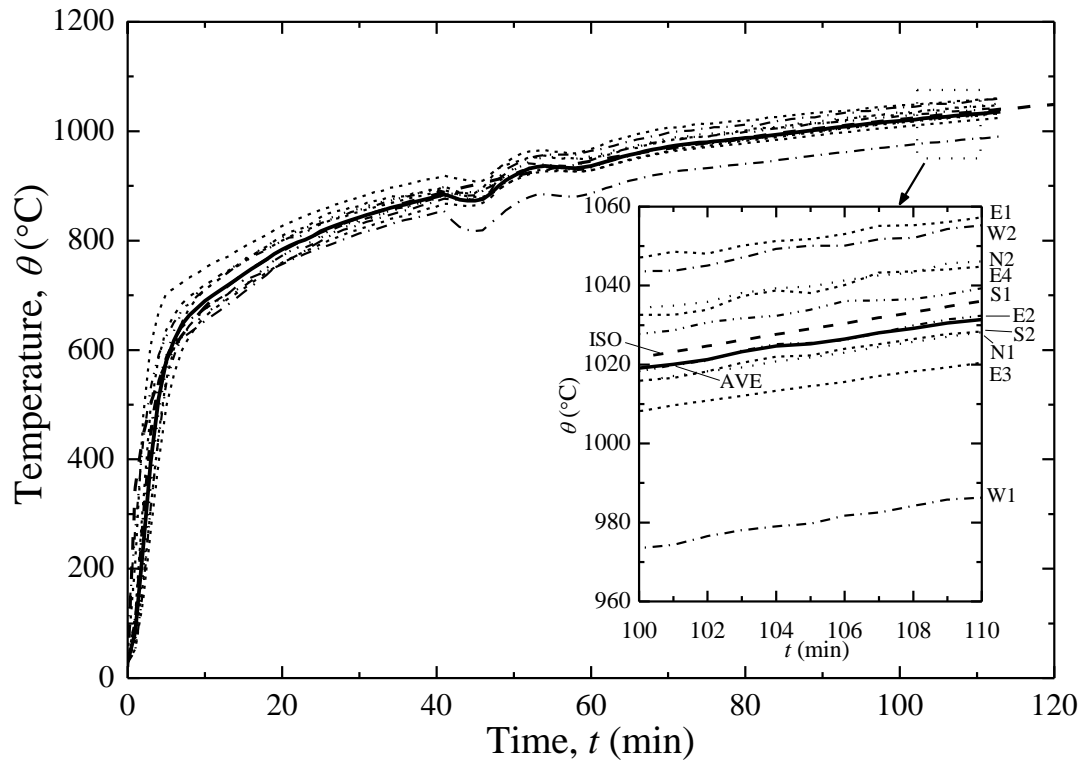
(a) Specimen J0-1
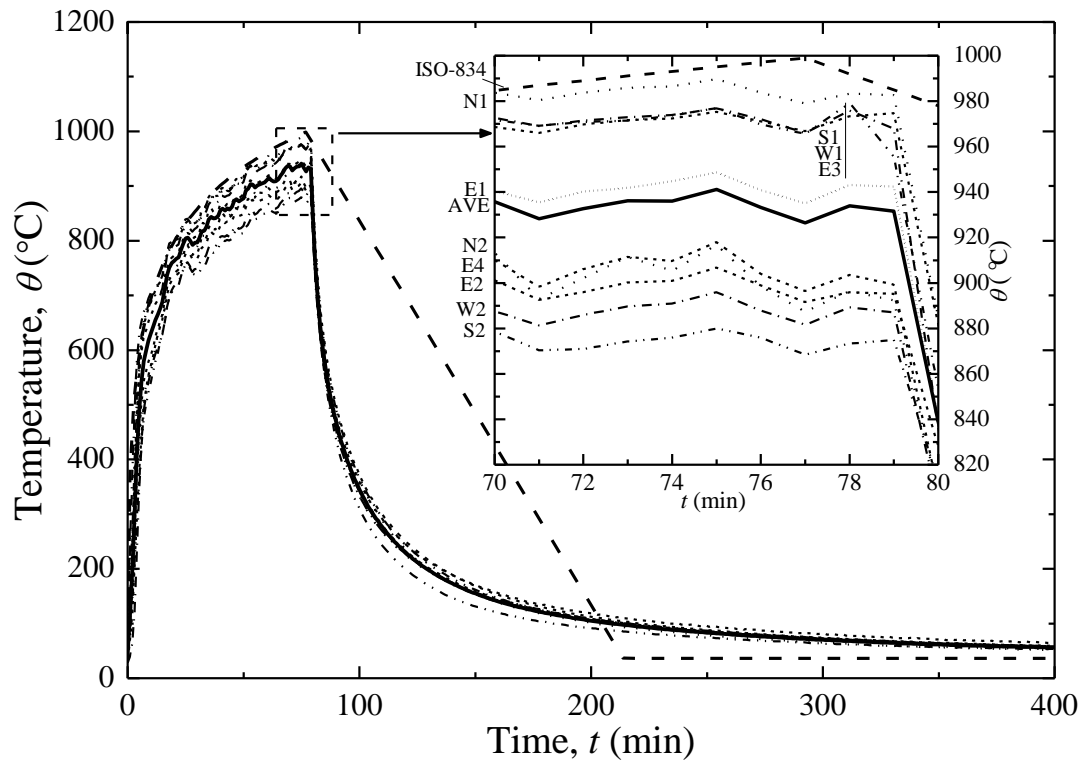
(b) Specimen J0-4

Fig. 7 Measured furnace temperature (θ) versus time (t) relationships.

9
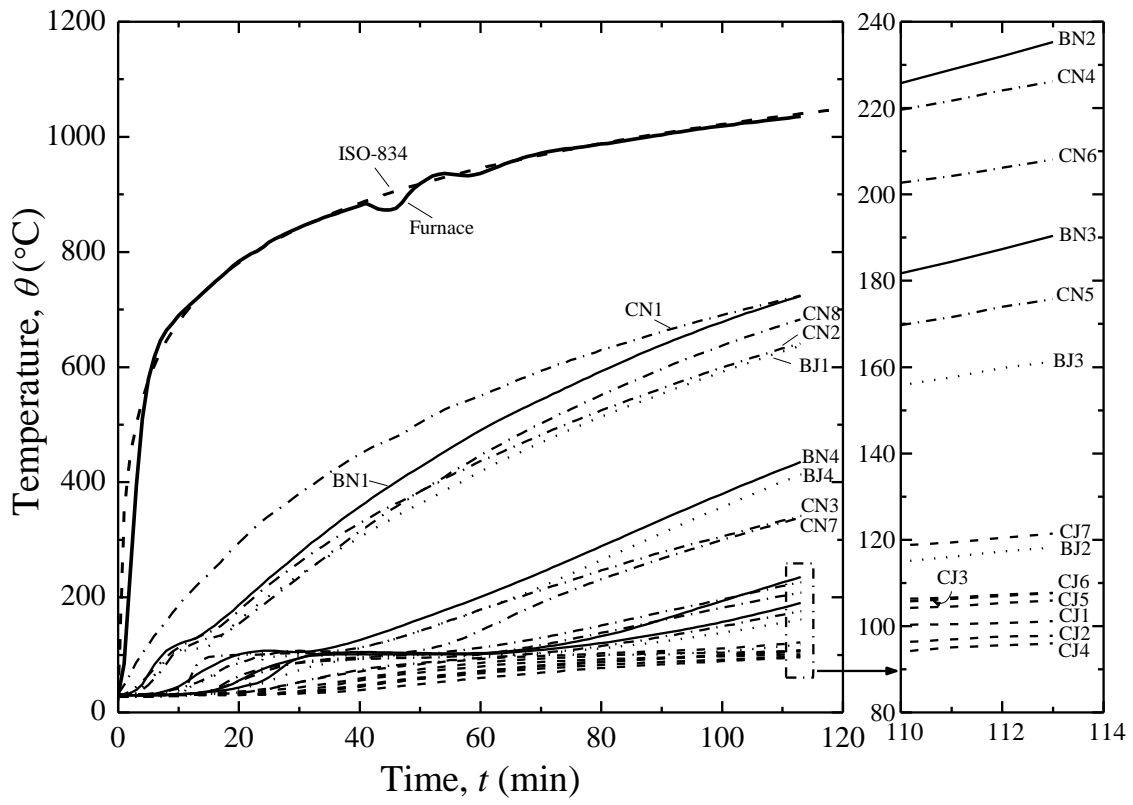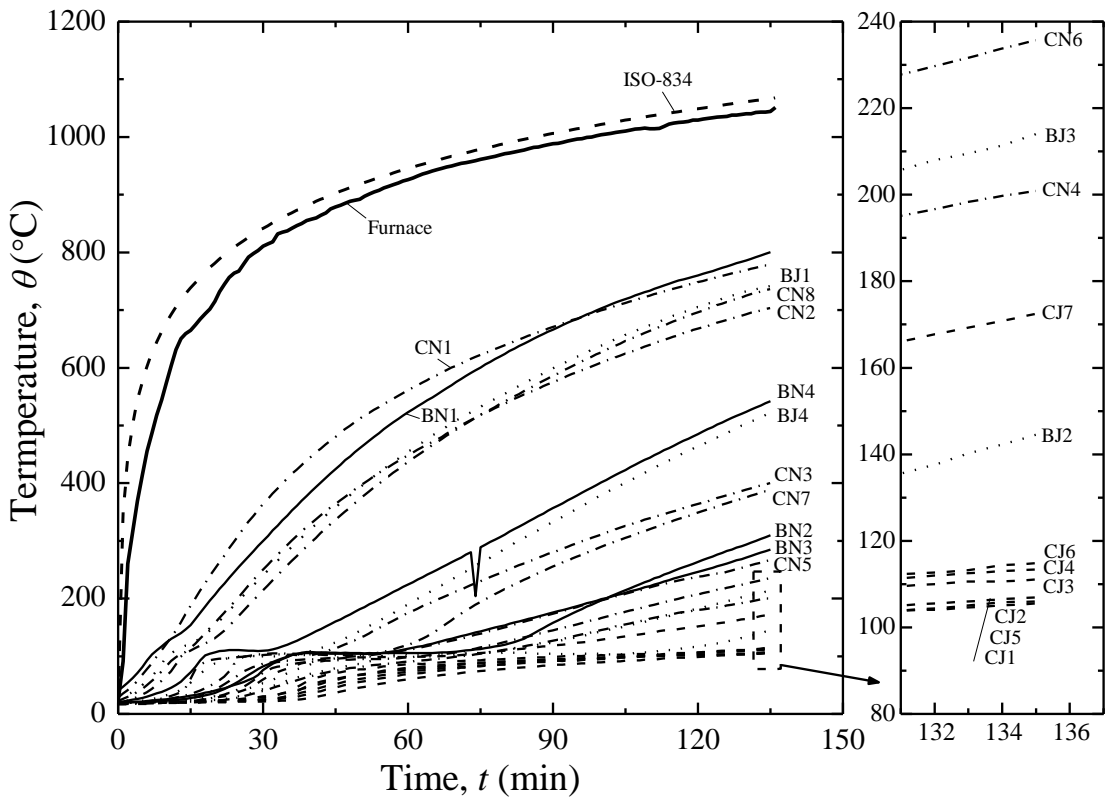
(a) Specimen J0-1

(b) Specimen J0-2
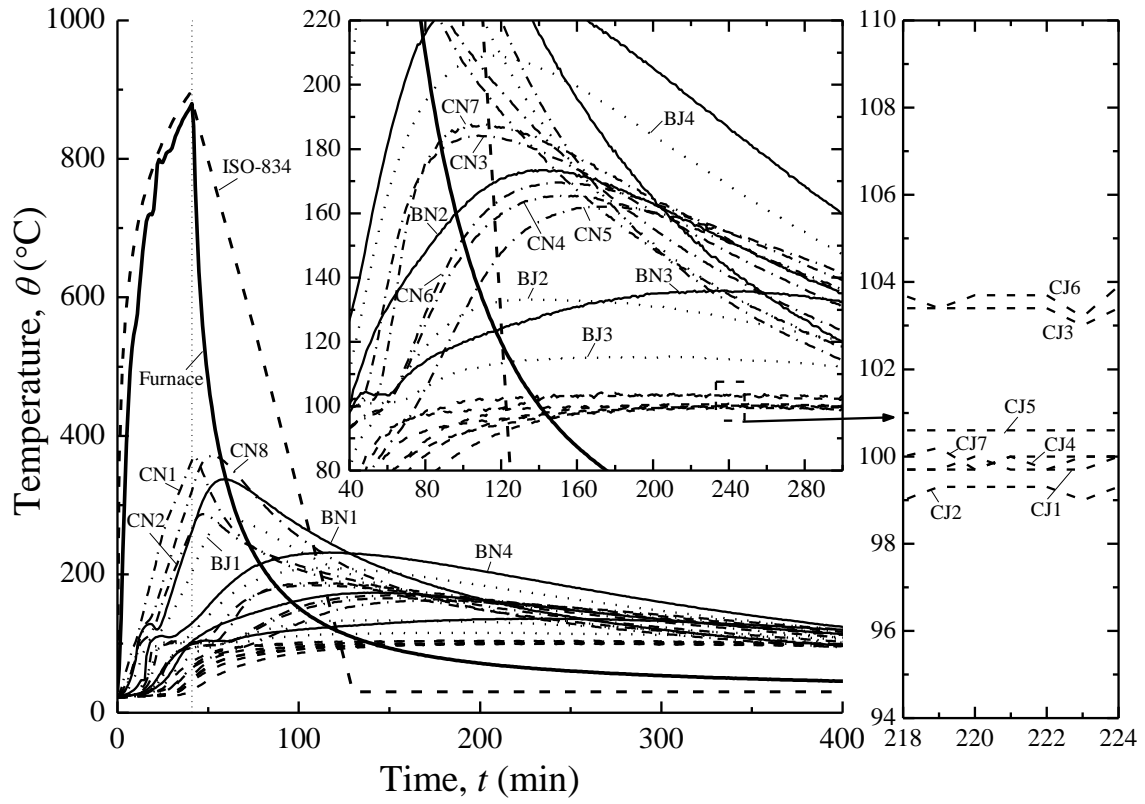
(c) Specimen J0-3

(d) Specimen J0-4

11
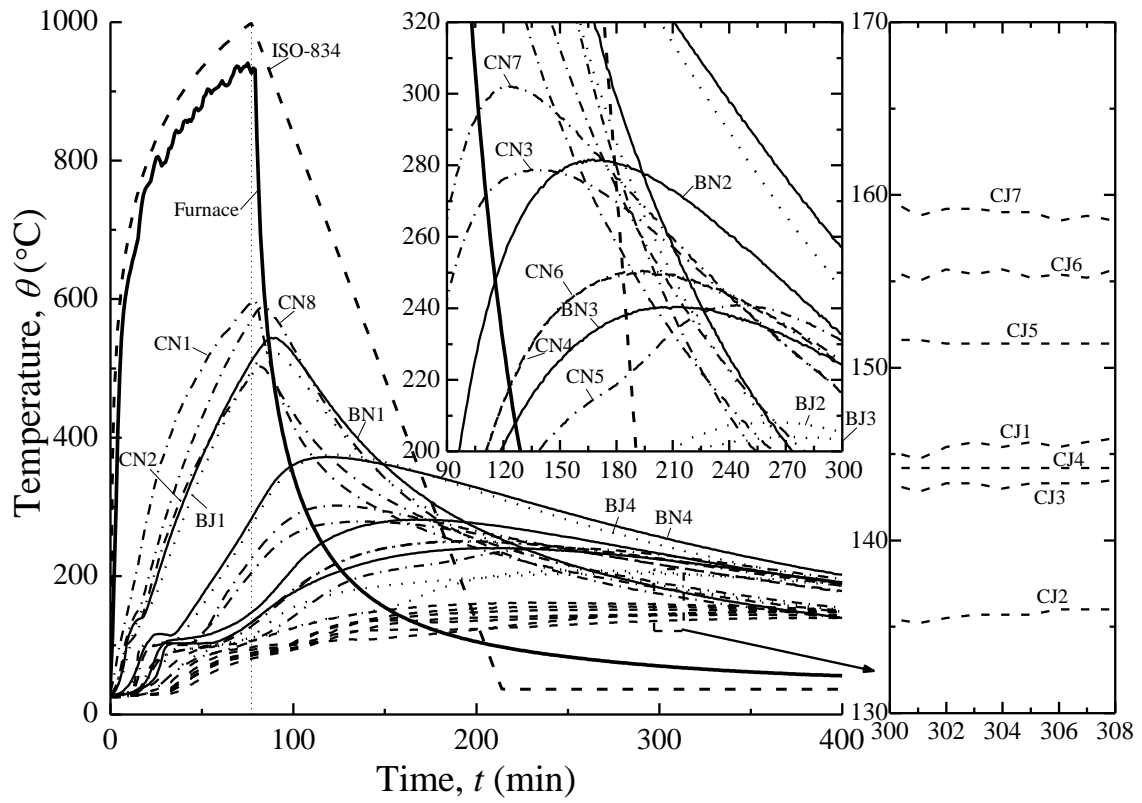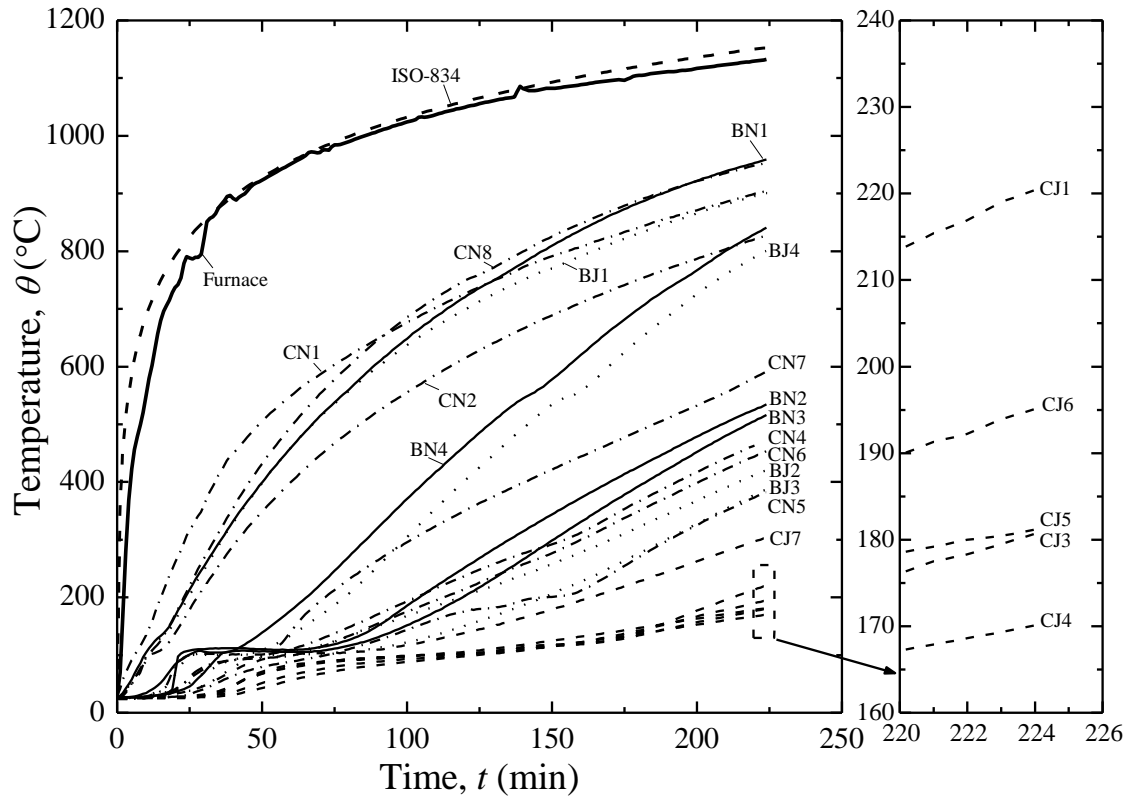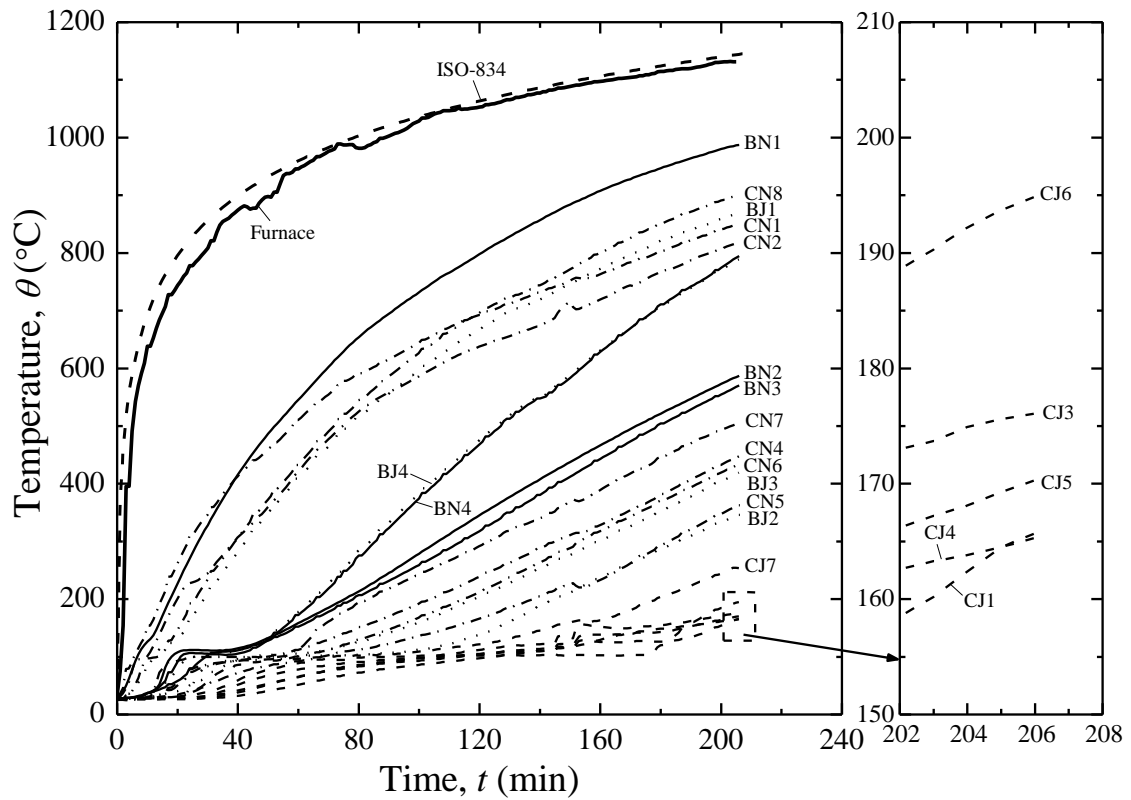
(e) Specimen J0-5

(f) Specimen J0-6

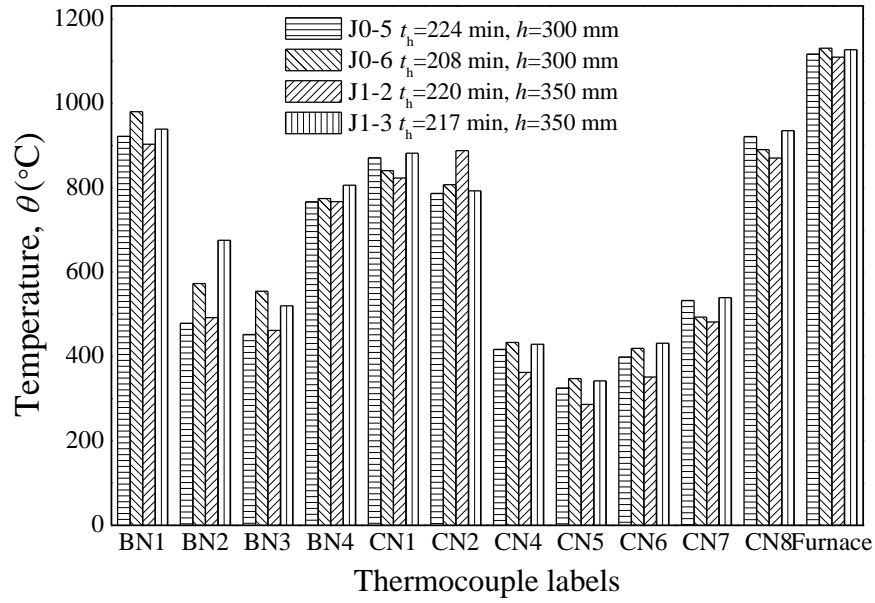Fig. 8 Measured temperature (θ) versus time (t) relationships of specimen group J0.

12
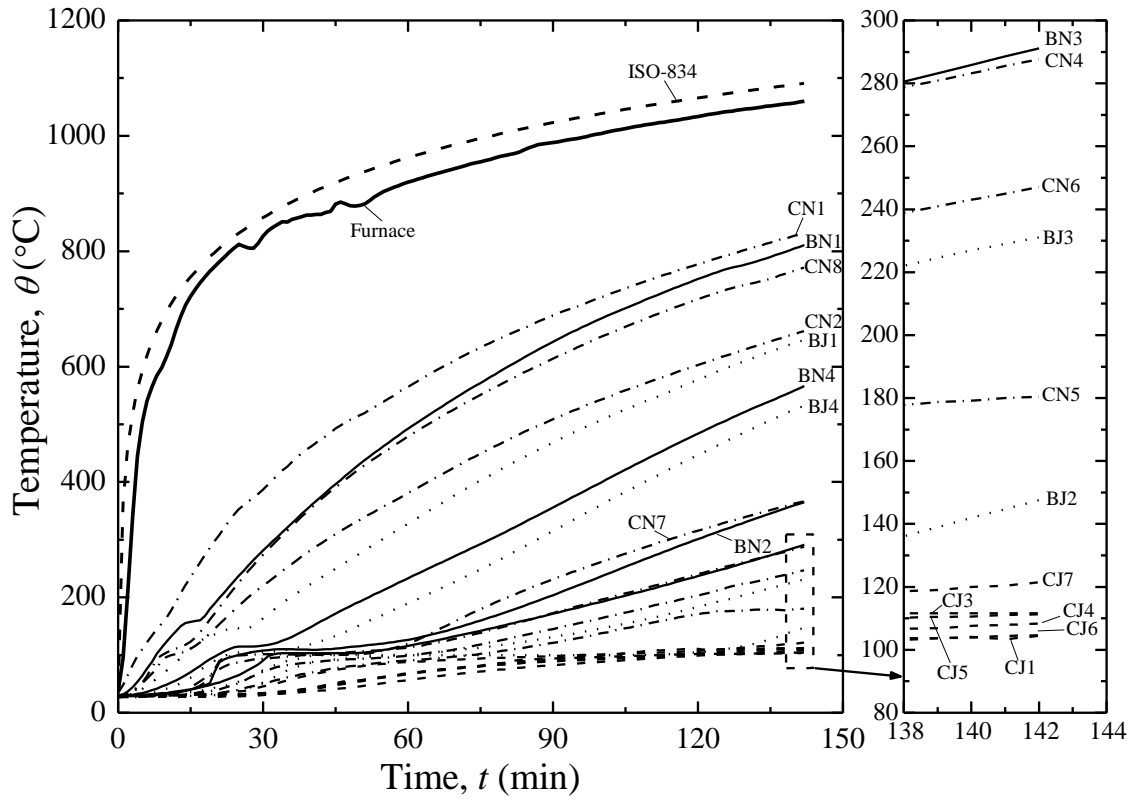
(a) Specimen J1-1

(b) Specimen J1-2

13
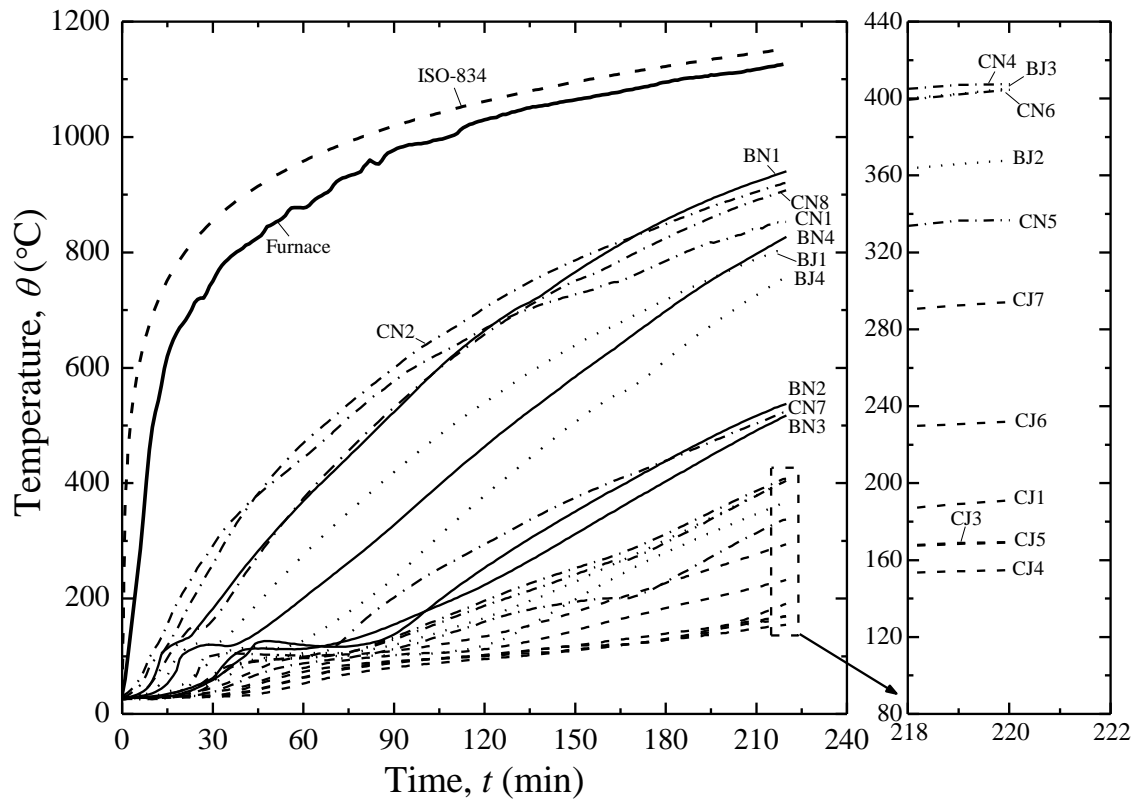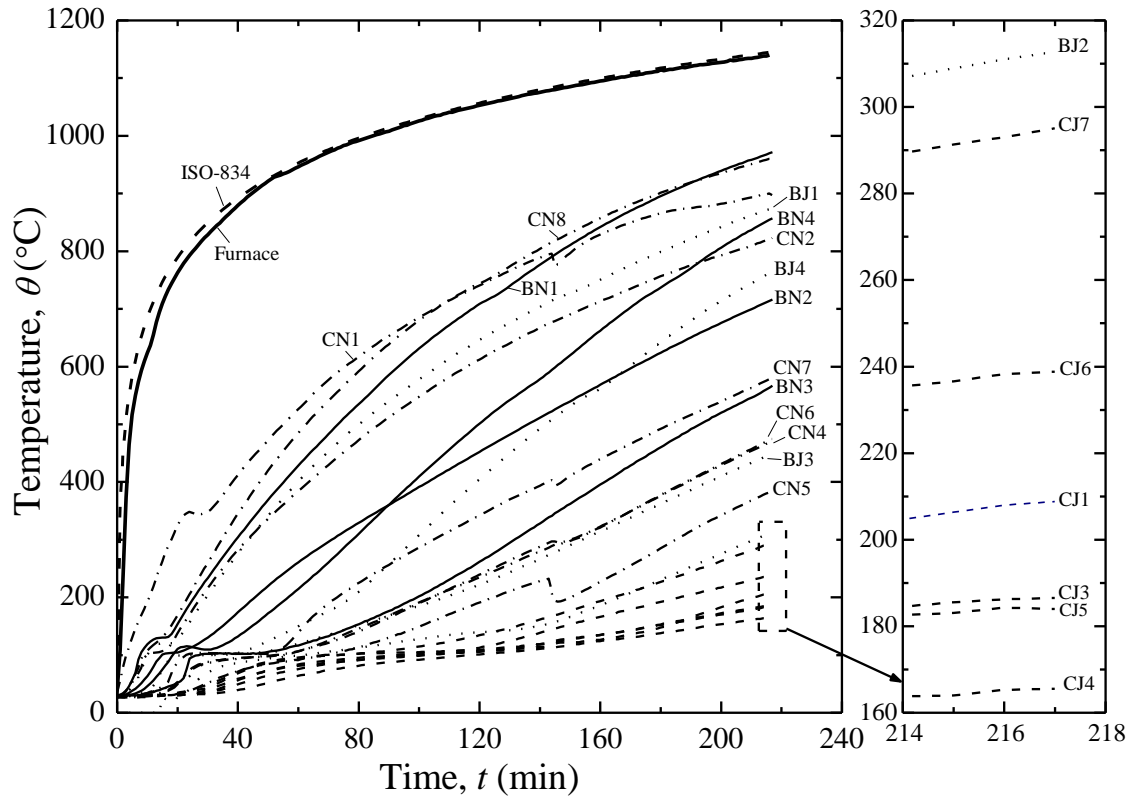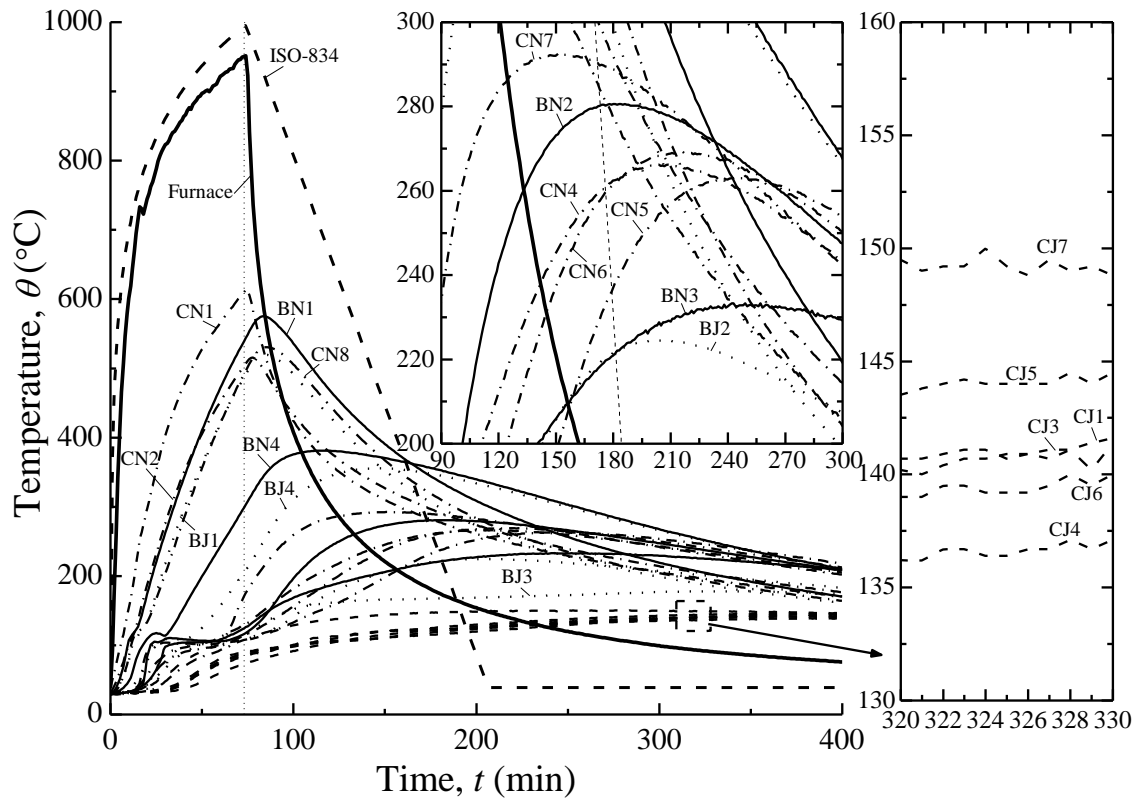
(c) Specimen J1-3

(d) Specimen J1-4

Fig. 9 Measured temperature (θ) versus time (t) relationships of specimen group J1.

14
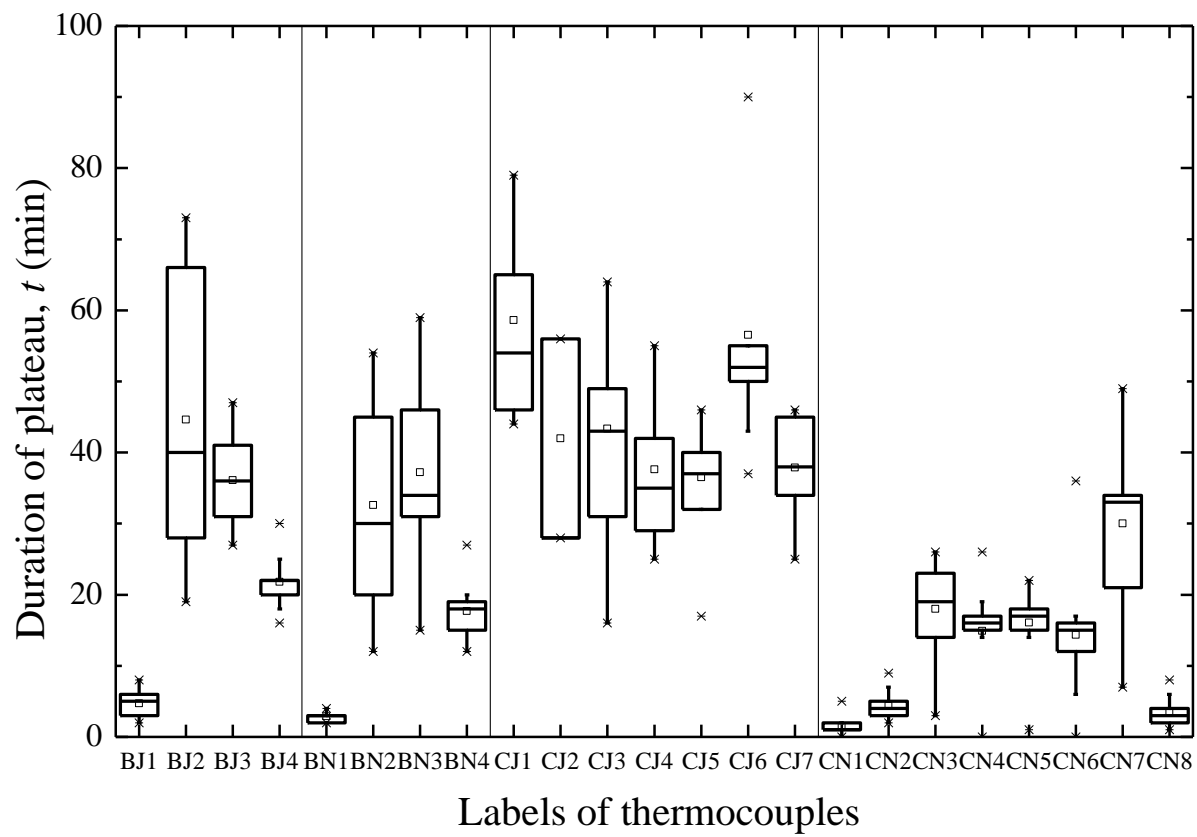
Fig. 10 Duration of moisture plateau.
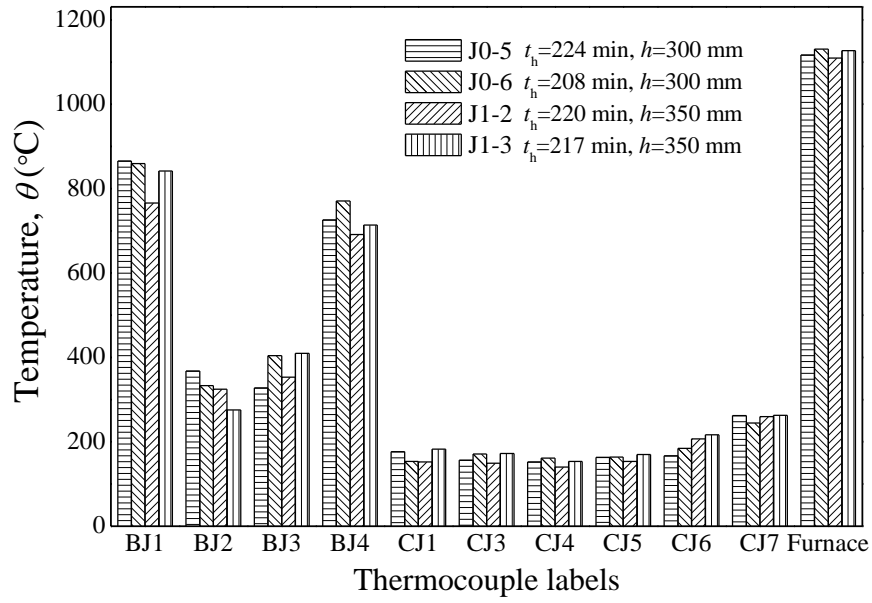
(a) Joint zone

(b) Non-joint zone

Fig. 11 Effect of beam height h on temperature θ (temperature at 200 min is extracted).
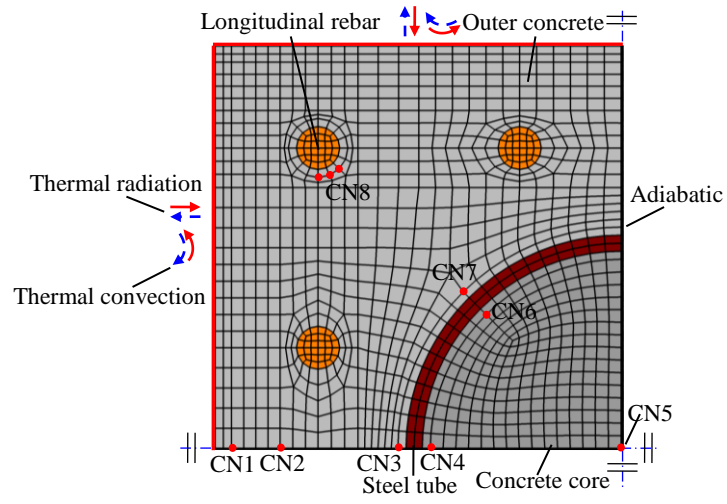
(a) Meshing of a quarter of cross-section CN (column).
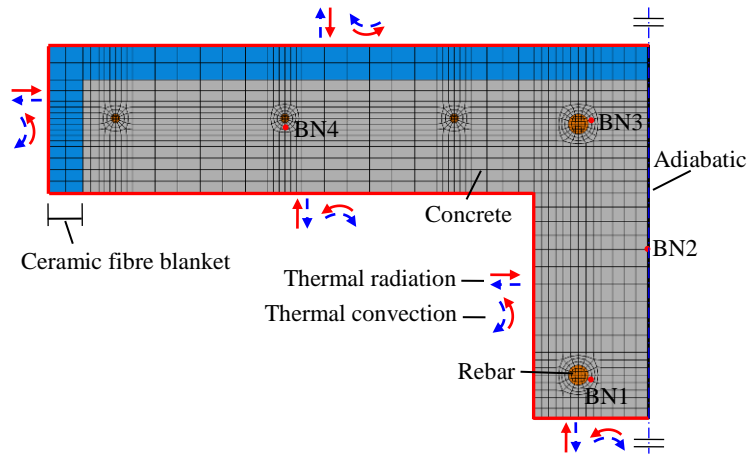
(b) Meshing of a half of cross-section BN (RC beam).

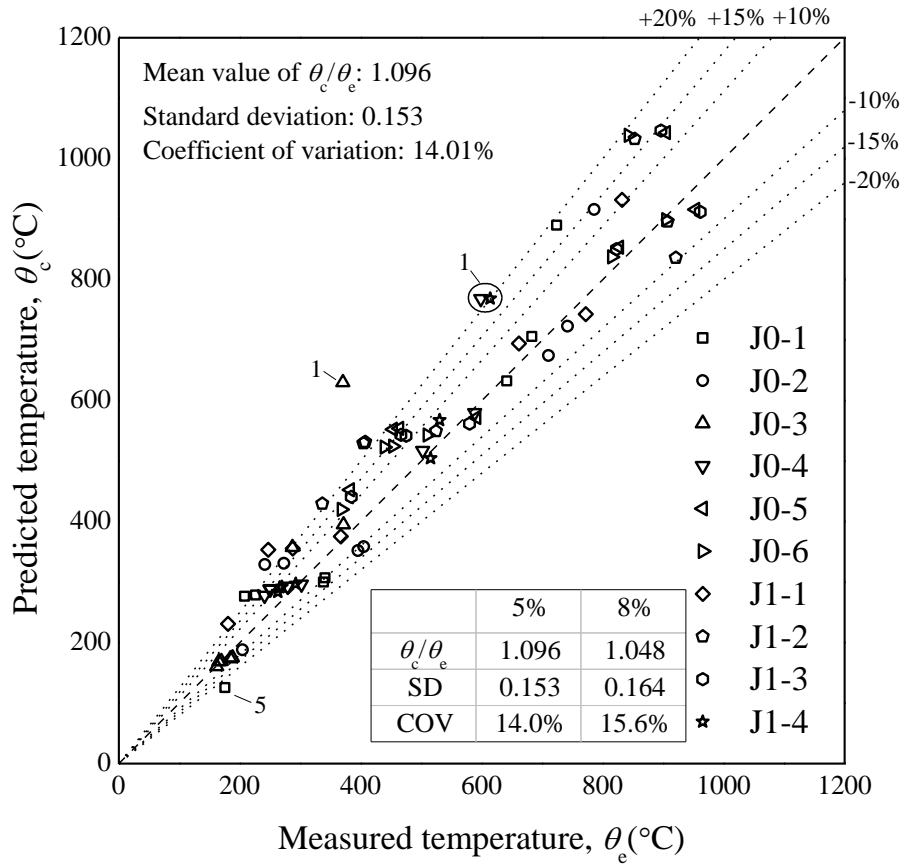Fig. 12 Two-dimensional (2D) heat transfer analysis models.
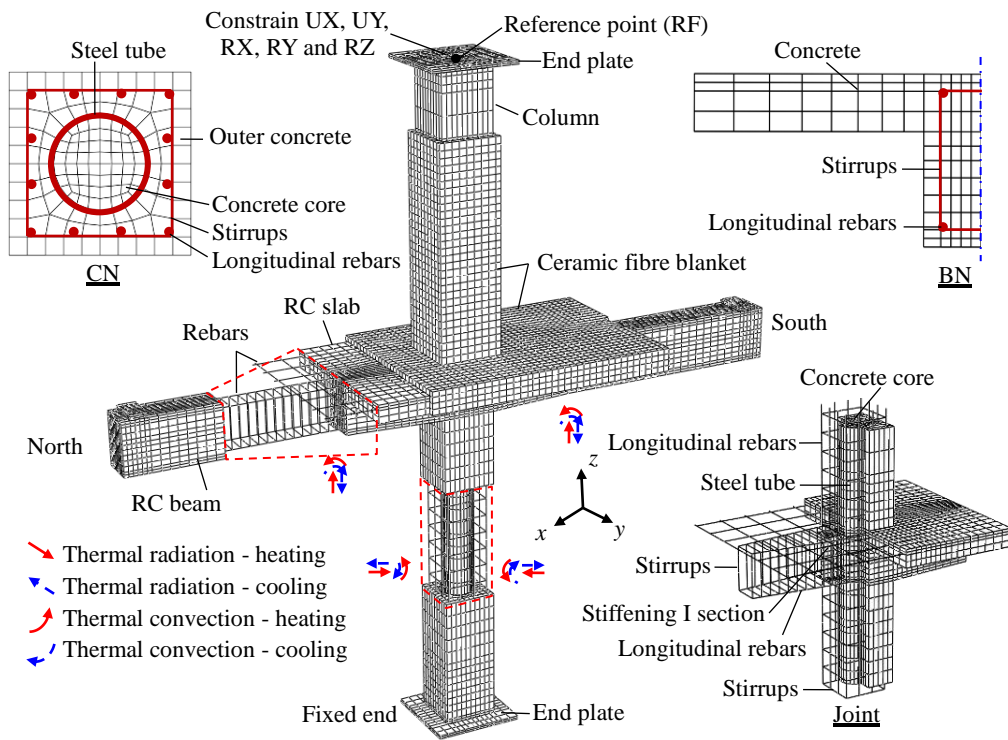
Fig. 13 Three-dimensional (3D) heat transfer analysis model.
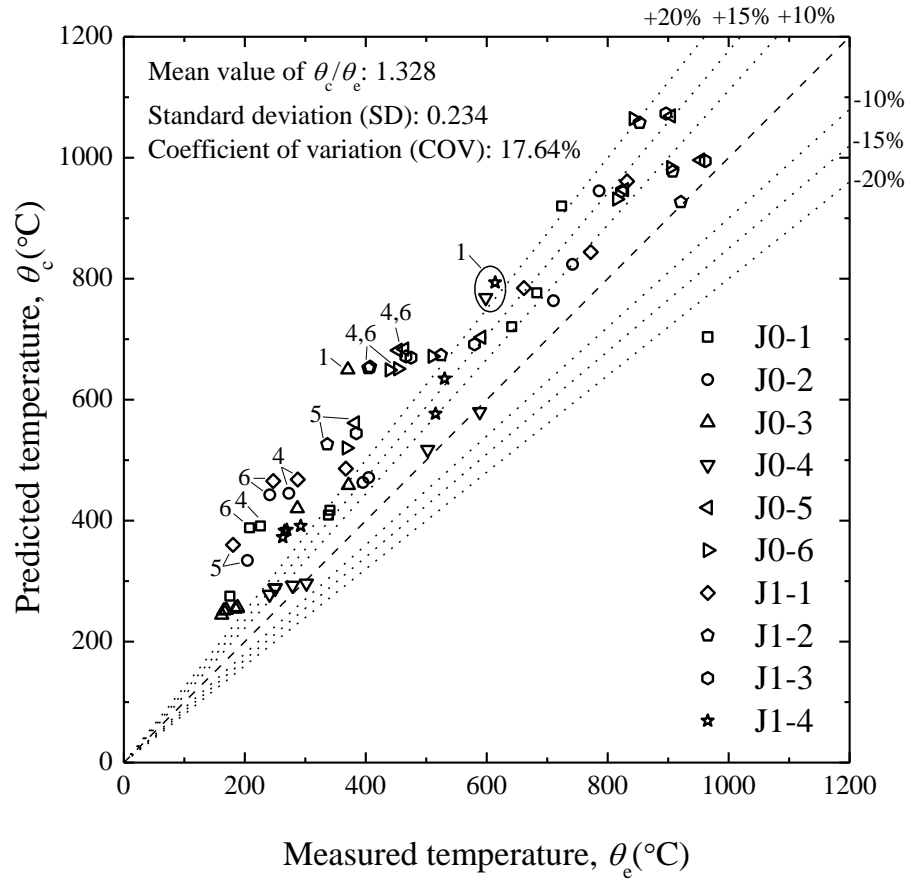
(a) Predicted versus measured temperatures (thermal properties: Lie [38])

(b) Predicted versus measured temperatures (thermal properties: Eurocode 4, u=5%)
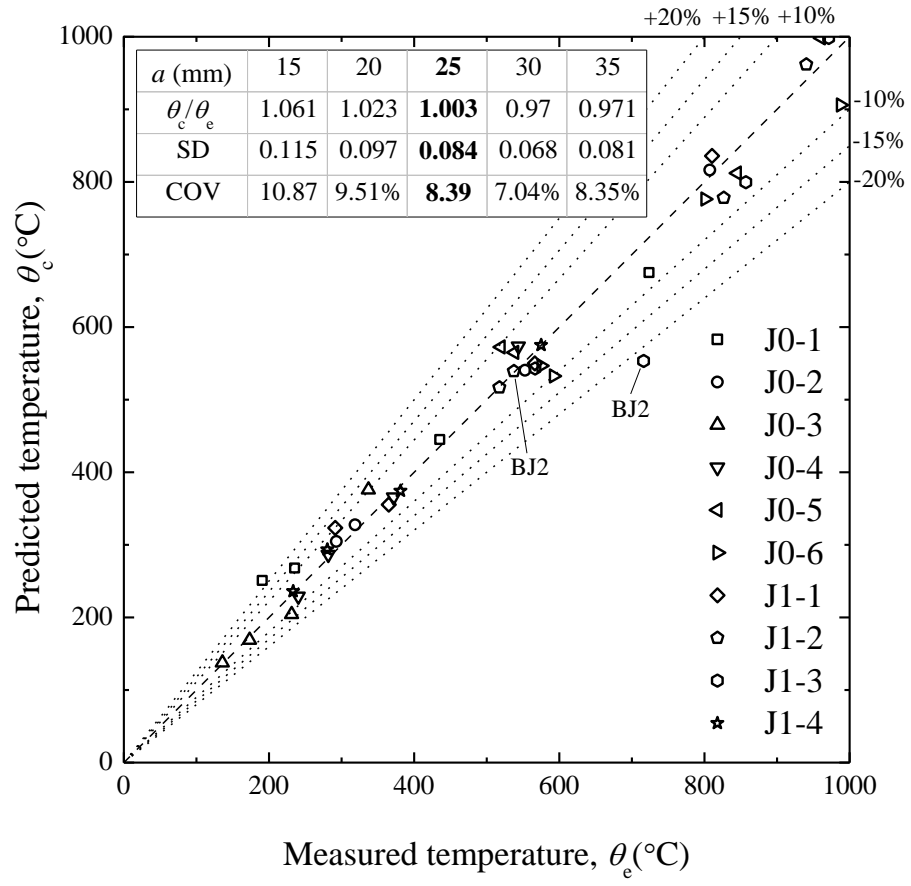Fig. 14 Comparison between predicted and measured temperatures for cross-section CN.

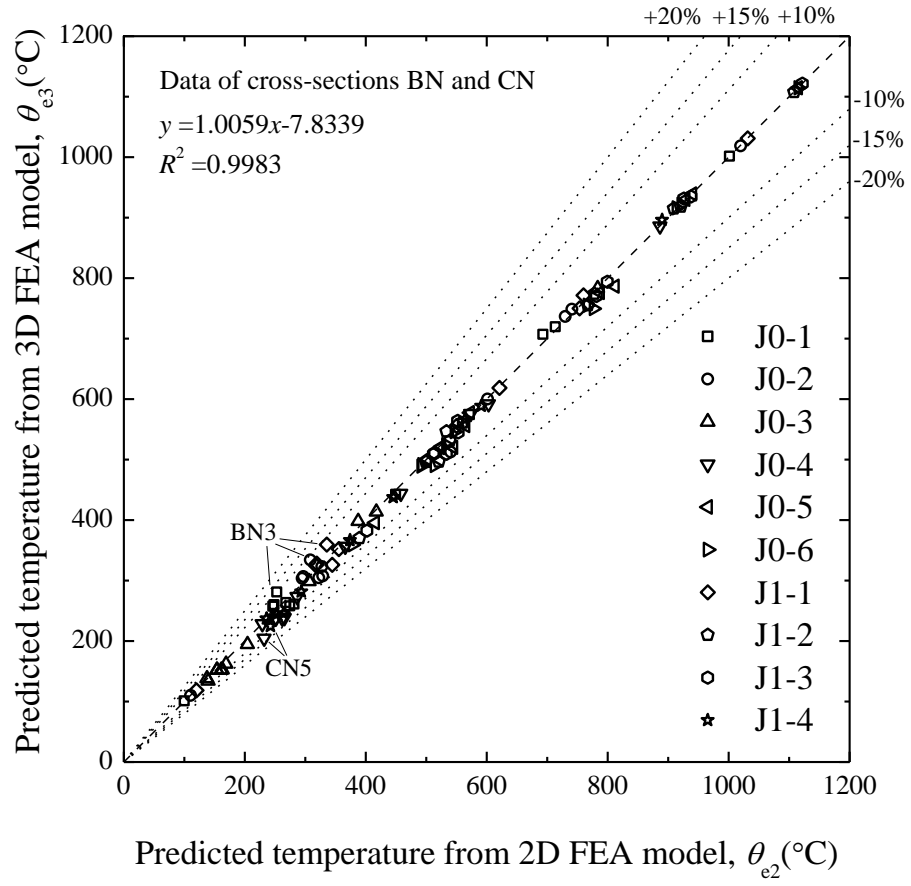Fig. 15 Comparison between predicted and measured temperatures for cross-section BN (*a*=25 mm).
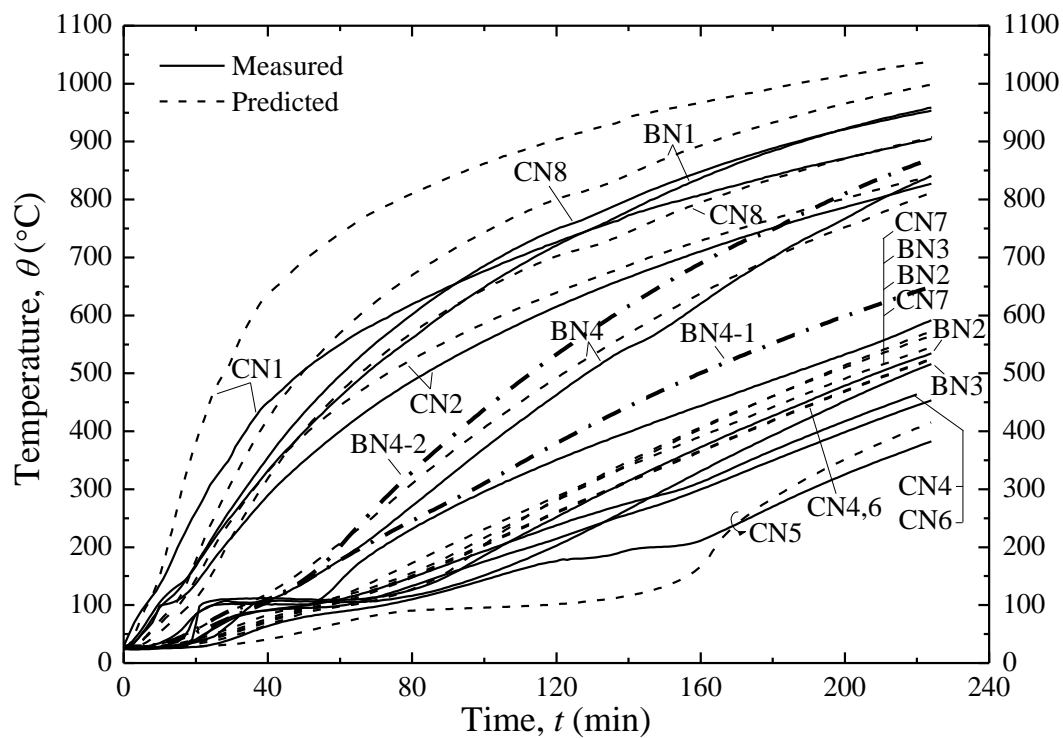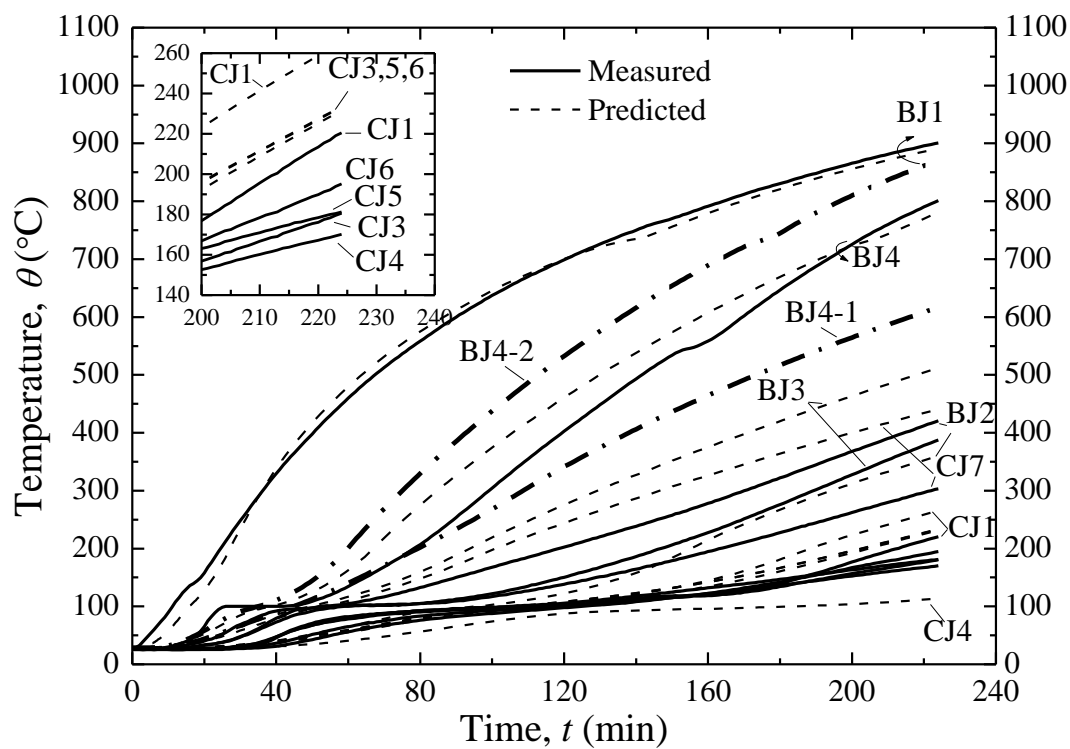
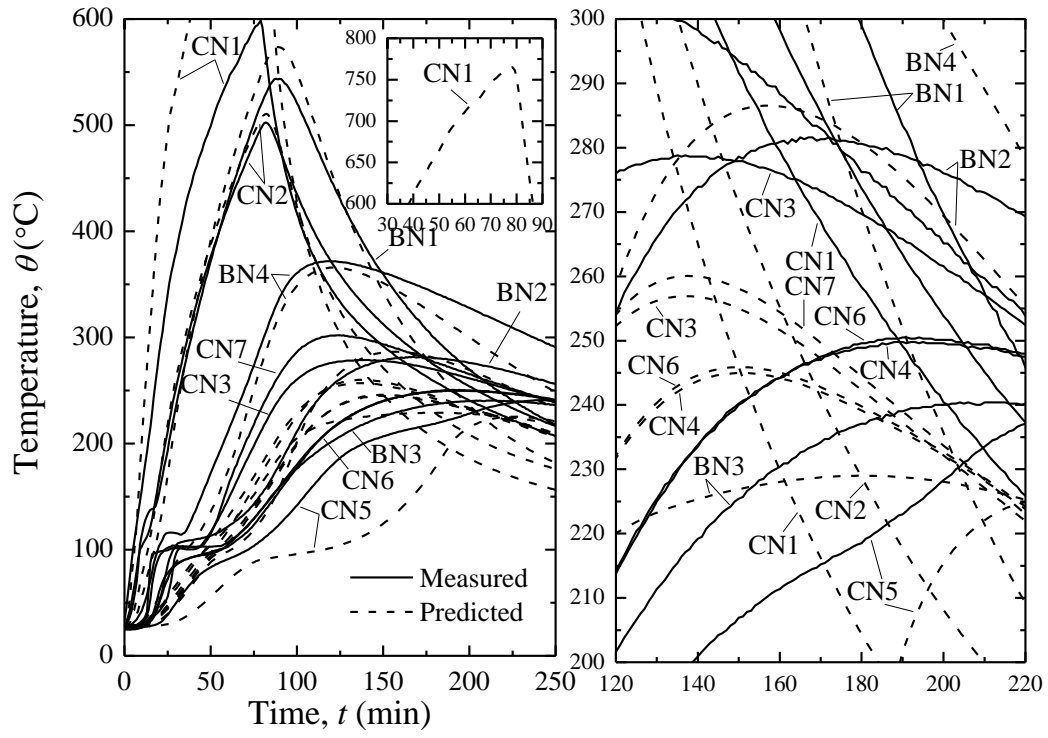Fig. 16 Comparison of temperatures obtained from 2D and 3D FEA models.
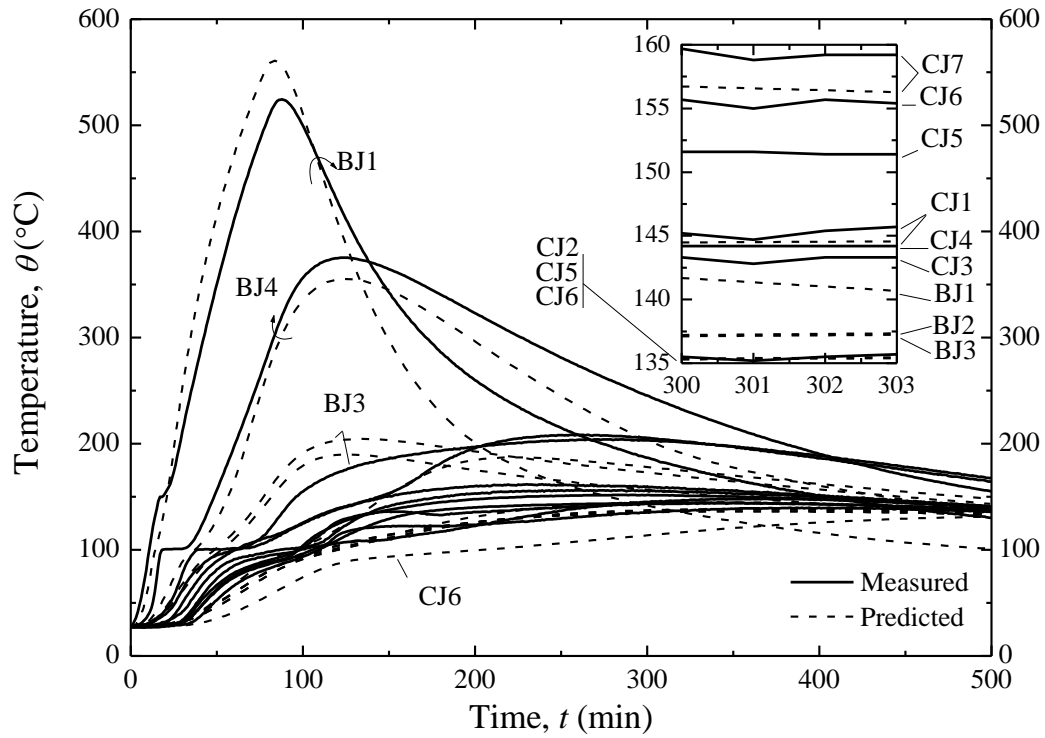
(a) Thermocouples BN and CN

(b) Thermocouples BJ and CJ

Fig. 17 Temperature (θ) versus time (t) relationships of Specimen J0-5 (fire resistance test).

(a) Thermocouples BN and CN

(b) Thermocouples BJ and CJ

Fig. 18 Temperature (θ) versus time (t) relationships of Specimen J0-4 (post-fire test).

23

Captions for tables

Table 1 Summary of test information and results.

Label	$B_c \times D_c$ (mm) $D \times t_s$ (mm) $h \times b$ (mm)	Column load, N_f (kN)	Beam load, P_f (kN)	Fire resistance, t_R (min)	Heating time, t_h (min)	Heating time ratio, t_o	Test type[1]	Failure Type[2]
J0-1		2036	46.30	110	113	1.02	R	B(S, N)
J0-2	□	2071	42.30	116	135	1.16	R	B(N, S)
J0-3	−300×300	2071	42.30	-	41	0.36	P	B
J0-4	○−159×6	2071	42.30	-	77	0.68	P	B
J0-5	300×200	2071	23.15	217	224	1.03	R	B(S, N)
J0-6		1450	23.15	200	208	1.04	R	B(S, N)
J1-1	□	2071	53.10	121	142	1.17	R	B(N, S)
J1-2	−300×300	2071	26.50	214	220	1.03	R	B(N, S)
J1-3	○−159×6	1450	26.50	217	217	1.00	R	B(N)
J1-4	350×200	1450	26.50	-	72	0.33	P	B

1. In test type, 'R' denotes fire resistance test and 'P' denotes post-fire test.

2. In failure type, 'B' denotes the two beams failed simultaneously. 'B(S, N)' denotes both the south and the north beam failed, but the south beam failed prior to the failure of north beam. 'B(N)' means the north beam failed but the south beam did not fail until the end of test.

Table 2 Strength of concrete

Type	28 days			589 days for infilled concrete/574 days for outer concrete		
	Cube strength, N/mm^2	Number of samples	SD, N/mm^2	Cube strength, N/mm^2	Number of samples	SD, N/mm^2
Infilled concrete	56.4	6	5.43	61.4	6	4.24
Outer concrete	24.9	4	4.11	31.8	4	3.28

Table 3 Material properties of steel tube and reinforcement.

Materials	D (mm)	f_y (N/mm^2)	f_u (N/mm^2)	E_s (N/mm^2)	v_s
Steel tube	159	416	642	245,000	0.279
Steel plate (end plates)	10	374	515	228,000	0.275
Longitudinal reinforcement in beam	18	412	581	201,000	0.294
Longitudinal reinforcement in column	16	363	558	190,000	0.296
Stirrups (for both beam and column)	8	284	471	217,000	-